The effect of elastic couplings and material uncertainties on the flutter of composite high aspect ratio wings

M.R. Amoozgar [1], R.M. Ajaj [2], J.E. Cooper[3]

[1] *Faculty of Engineering, University of Nottingham, Nottingham, NG7 2RD, United Kingdom*

[2]*Department of Aerospace Engineering, Khalifa University of Science and Technology, Abu Dhabi, UAE*

[3] *Department of Aerospace Engineering, Bristol University, Bristol, BS8 1TR, United Kingdom*

Abstract

In this paper, the stochastic aeroelastic stability analysis of a composite high aspect ratio wing with various elastic couplings is investigated. The wing consists of a rectangular spar-box made from composite materials. Due to its high aspect ratio, the wing structure is modelled using the exact beam formulation, and the aerodynamic loads acting on the wing are simulated using an unsteady lifting line theory. A composite spar-box cross section is considered, and the effect of various effective parameters on the aeroelastic stability of the wing is studied. First, a baseline composite wing is designed and the effect of three different elastic couplings on the stability of the wing is determined. These three elastic couplings that affect the aeroelastic design of the composite wing are the out-of-plane (flap)-twist, the in-plane (lag)-twist and the extension-twist. Furthermore, the effect of uniformly distributed load on the aeroelastic stability of the wing is assessed for various layups. Finally, the effect of material uncertainties on the aeroelastic stability of the composite wing with various couplings is studied. It is observed that the type of elastic coupling has a significant effect on the sensitivity of the flutter speed and frequency of the composite wing due to the randomness of the material properties. In particular, the aeroelastic behaviour of the wing with lag-twist coupling is more sensitive to the material uncertainties than other two layups.

Keywords: Aeroelastic stability, high aspect ratio wing, elastic couplings, material uncertainties.

Nomenclature

c = wing chord

U_D = flutter speed

F, **M** = internal force, and moment

f, **m** = external forces and moments

H, **P** = linear and angular momenta

h_s = spar-box height

i = mass moment of inertia

k, K = initial, and final curvature vectors

l = wing length

S = Stiffness matrix

t_s = spar-box thickness

U = free stream velocity

U_f = flutter speed

V, Ω = linear and angular velocity

w_s = spar-box width

y_{ac} = offset between aerodynamic centre and beam reference axis

γ, κ = generalized strains

ω_f = flutter frequency

θ = ply angle

μ = mass per unit length

x_2, x_3 = mass offset from reference coordinate

λ = inflow

Introduction

Due to their promising aerodynamic performance ([1]), high aspect ratio wings have drawn a huge interest in the last decade. One of the first proposed concepts for an aircraft with high aspect ratio wings is the High Altitude Long Endurance (HALE) aircraft [2, 3]. Although increasing the aspect ratio of the wing significantly increases

the lift to drag ratio through the reduction of lift induced drag, wing aeroelastic instabilities can become a major concern. Structural nonlinearities due to the large deformation of the wing have a major influence on the aeroelasticity behaviour of high aspect ratio wings compared to conventional designs [4, 5]. It has been shown that using linear structural models result in an inaccurate prediction of aeroelastic stability for high aspect ratio wing ([6-8]). Hodges and Dowell [9] showed that for high aspect ratio structures (such as helicopter blades), modelled with beam elements, it is likely that the flap, lag and torsion modes couple due to the existence of strong nonlinearity in the system. Patil et al. [10] studied the nonlinear aeroelasticity of a HALE aircraft in subsonic flow using the geometrically exact beam formulation; they showed that the large deformation nonlinearities of the structure result in different aeroelastic and trim behaviour of the aircraft compared with a linear aeroelastic model. Tang and Dowell [11] experimentally studied the aeroelasticity of high aspect ratio wings, comparing experimental results with a numerical model developed by combining a beam model with the ONERA stall model. They concluded that the lag to flap stiffness ratio is the key to decide whether to use a linear or nonlinear model for aeroelasticity modelling of wings. Their work has continued by considering the effect of gusts on the aeroelastic response of high aspect ratio wings [12]. Limit cycle oscillations of high aspect ratio wings (which can be due to nonlinear geometric effects or stall condition [13]) simulated using large deformation beam models has been investigated by Patil et al. [6]. It has been observed that, depending on the initial and stall conditions, the wing might experience various responses with different amplitudes. Also, they highlighted that the limit cycle oscillation might occur before the linear flutter speed. The effect of both structural and aerodynamic nonlinearities on the aeroelasticity of high aspect ratio wings has been discussed by Patil and Hodges [4] where it has been determined that the structural nonlinearity is more important than the aerodynamic nonlinearities. This work then extended by Amato et al. [14] to study the effects of wing large deformation on the frequencies and stability of the wing experimentally. Several other studies considered the aeroelasticity of high aspect ratio wings, reviewed by Afonso et al. [1]. More recently, Duan and Zhang [15] considered the aeroelastic stability of high aspect ratio wings using the transfer function method. Their proposed method was insensitive to the mesh density and did not require any structural modal analysis. Hoseini and Hodges [16] studied the aeroelastic stability of damaged high aspect ratio wings. They showed that the stability of the wing is sensitive to both the intensity and location of the damage. The nonlinear aeroelastic and gust response of high aspect ratio wings with geometrical nonlinearities has been considered by An et al. [17] where it was concluded that the geometric nonlinearities of the wing significantly affect the aeroelastic behaviour of an aircraft with high aspect ratio wings.

Due to their high specific strength and stiffness, composite materials have been widely used in aerospace structures ([18-25]). Liu and Xiang [26] considered the aeroelastic behaviour of high aspect ratio wings considering the stiffness coupling due to composite anisotropy. They showed that the flap-twist coupling of the composite lamination affects the onset of stall flutter of the wing. The aeroelasticity of composite high aspect ratio wings modelled using an exact beam formulation has been considered by Cesnik et al. [27] where a composite spar-box with flap-twist coupling has been considered, and the effect of various ply angles on the instability of the wing has been assessed. Baets et al. [28] looked at the aeroelastic behaviour and flutter speed sensitivity of composite spar-box wings with root flexibility; they observed that wing's root flexibility significantly affects its stability and can change both flutter and divergence speeds. The effect of combined twisting and bending actuation on the aeroelasticity of composite high aspect ratio wings has been investigated by Cesnik et al. [29] where the nonlinear aeroelastic response of the wing with embedded anisotropic piezoelectric actuators was considered. They concluded that the orientation of the actuators has the tailoring effect on the stability of the wing. Wang et al. [30] optimised the structure of a composite wing using an equivalent finite element model using a three-step optimisation process and the displacement, buckling, stiffness and aeroelastic stability requirements have been considered in the optimisation process. The nonlinear aeroelastic analysis of composite wings using moderate deflection beam theory combined with an unsteady aerodynamic model has been considered by Koohi et al. [31], and it was concluded that the shear deformation and composite material coupling terms are important in the aeroelastic analysis of composite wings. Amoozgar et al. [32] investigated the effect of wing pre-twist angle on the stability of tailored wings modelled by the exact beam formulation and showed that the wing's stability is sensitive to the magnitude and order of twist distribution. A further study then continued by considering the effect of wing curvature on the flutter stability of wings [33]. Finally, Amoozgar et al. [34] studied the effect of various elastic couplings on the vibration of composite rotating blades with curved tips and showed that the depending on the type of elastic coupling, the blade might experience different dynamic behaviours.

Although the numerical tools used for analysing the behaviour of composite structures have evolved in the recent two decades to increase the modelling accuracy, in reality the manufacturing processes are subjected to uncertainties. These variabilities occur due to the manufacturing process and/or time degradation can alter the properties of the structure, and therefore they need to be considered carefully. Previous studies have considered the effect these uncertainties on the behaviour of composite structures behaviour. For example, Pettit [35] showed that the properties of a scaled manufactured blade are different from the pre-designed values due to the variations in the manufacturing processes with the material properties of composite structures being subjected to

uncertainties due to the randomness of ply angle, ply thickness, curing process, fibre volume, fibre and matrix material properties, voids, fibre and resin rich areas, and fibre undulation ([36, 37]). Although the amount of variation in material properties cannot be known as a-priori, Onkar et al. [36] suggested that the coefficient of variation of the module of elasticity of a lamina can vary within the range of 5% to 15%. Lindsey et al. [38] studied the effect of uncertainties in material properties and boundary conditions on the nonlinear aeroelasticity of panels in supersonic flow. They showed that uncertainties affect the limit cycle oscillation amplitude of the panel significantly. Murugan et al. [39] studied the effect of randomness of material properties on the aeroelastic response and stability of composite blades and showed that the aeroelastic behaviour of the blade with material uncertainties has considerable deviation from the baseline values. Borello et al. [40] determined the effect of structural uncertainties on the aeroelastic stability of both isotropic and composite wings. They showed that the fast probabilistic methods might give nonconservative results in compare to Monte Carlo simulations. The effect of uncertainty on the aeroelastic stability of composite wings using Polynomial Chaos Expansion was considered by Scarth et al. [41] who showed that their proposed method for uncertainty quantification reduces the computational time by one order of magnitude when compared to the Monte Carlo simulation. Also, they found that the ply angle uncertainty can cause variations in bend-twist coupling which might result in switch in response mechanism. The effect of uncertainty of ply angle and ply thickness on the flutter speed of a composite plate has been determined by Nitschke et al. [42]. The polar method was used to reduce the set of stochastic parameters and it was observed that the manufacturing tolerances change the flutter speed of the plate particularly when mode switching happens. More recently, Adamson et al. [43] studied the uncertainty quantification of aeroelastic systems by modifying the measured receptance data. The advantage of this uncertainty quantification method was that it removes the need to model the aerodynamics or structure explicitly, and hence avoided the numerical or model uncertainties. Guimaraes et al. [44] investigated the effect of uncertainties of the fibre volume on the aeroelastic stability of tow-steered composite plates, employing a new and efficient computational method for uncertainty analysis. It is noted that, to the best of the authors' knowledge, the combined effects of material uncertainties and various elastic couplings on the aeroelastic stability of high aspect ratio wings have not previously been investigated.

This study expands the above literature by considering the effect of uncertainties on the aeroelastic stability of composite high aspect ratio wings (HARW) with three elastic couplings. A baseline composite wing with a rectangular spar-box has been introduced, and the effect of ply angle on the stability of the wing is determined. Three types of elastic couplings are considered which are the extension-twist, lag-twist and flap-twist. Finally, the

effects of distributed load (due to inertial load/acceleration) and material uncertainties on the nonlinear flutter speed and frequency of the composite wing with various ply angles and elastic couplings are investigated.

Mathematical Model

A composite high aspect ratio wing, as shown in Figure 1, is considered. The spar of the wing is assumed to be a rectangular composite box fitted in the wing. The inner height, inner width and wall thickness of the spar box are denoted by h_s, w_s ,and t_s respectively. The spar-box consists of 6 layers of composite materials each with a ply angle of θ as shown in Figure 2. The length of the wing is *l* and the chord length is *c*. Three layup configurations have been considered here. In the first case, an anti-symmetric layup is considered where the extension-twist coupling is dominant, while in the other two symmetric cases, the flap-twist and lag-twist couplings are dominant. Finally, the nonlinear aeroelastic stability of composite high aspect ratio wings is investigated.

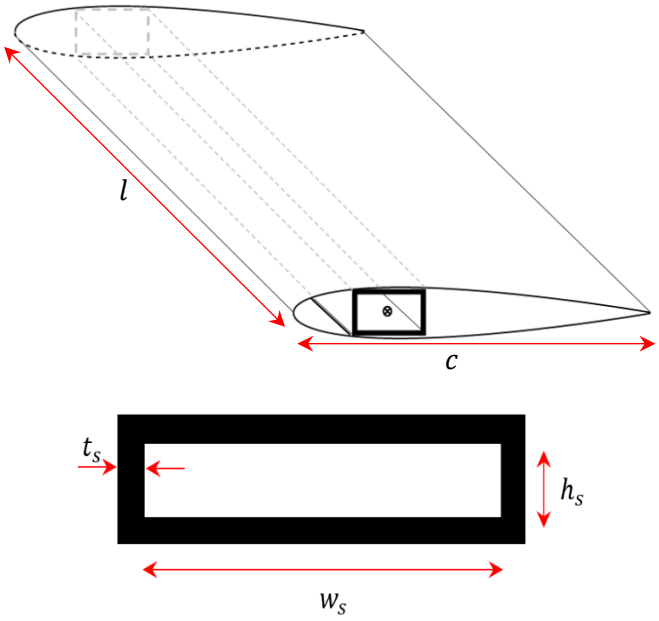

Figure 1: a) The wing cross-section b) the geometry of the composite spar-box

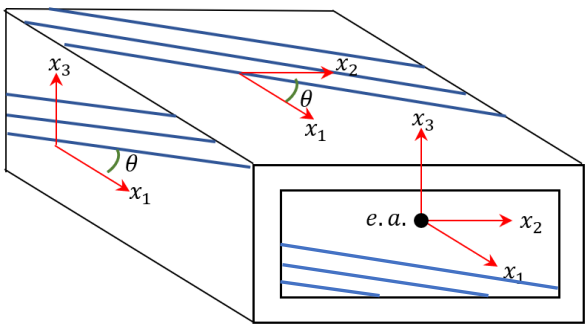

Figure 2: The composite spar-box layup sign convention

Aeroelastic Governing Equations

To govern the aeroelastic equations of a highly flexible wing, the geometrically exact fully intrinsic beam formulation [45] is used to take into account the structural dynamics of the wing. The exact fully intrinsic beam equations for a straight beam without any initial twist and curvature can be written as

$$
\begin{aligned}
&\partial F_1/\partial x_1 + \kappa_2 F_3 - \kappa_3 F_2 + f_1 = \partial P_1/\partial t + \Omega_2 P_3 - \Omega_3 P_2 \\
&\partial F_2/\partial x_1 + \kappa_3 F_1 - \kappa_1 F_3 + f_2 = \partial P_2/\partial t + \Omega_3 P_1 - \Omega_1 P_3 \\
&\partial F_3/\partial x_1 + \kappa_1 F_2 - \kappa_3 F_1 + f_3 = \partial P_3/\partial t + \Omega_1 P_2 - \Omega_2 P_1 \\
&\partial M_1/\partial x_1 + \kappa_2 M_3 - \kappa_3 M_2 + 2\gamma_{12} F_3 - 2\gamma_{13} F_2 + m_1 = \partial H_1/\partial t + \Omega_2 H_3 - \Omega_3 H_2 + V_2 P_3 - V_3 P_2 \\
&\partial M_2/\partial x_1 + \kappa_3 M_1 - \kappa_1 M_3 + 2\gamma_{13} F_1 - (1+\gamma_{11}) F_3 + m_2 = \partial H_2/\partial t + \Omega_3 H_1 - \Omega_1 H_3 + V_3 P_1 - V_1 P_3 \\
&\partial M_3/\partial x_1 + \kappa_1 M_2 - \kappa_2 M_1 + (1+\gamma_{11}) F_2 - 2\gamma_{12} F_1 + m_3 = \partial H_3/\partial t + \Omega_1 H_2 - \Omega_2 H_1 + V_1 P_2 - V_2 P_1 \\
&\partial V_1/\partial x_1 + \kappa_2 V_3 - \kappa_3 V_2 + 2\gamma_{12}\Omega_3 - 2\gamma_{13}\Omega_2 = \partial \gamma_{11}/\partial t \\
&\partial V_2/\partial x_1 + \kappa_3 V_1 - \kappa_1 V_3 - (1+\gamma_{11})\Omega_3 + 2\gamma_{13}\Omega_1 = 2\partial \gamma_{12}/\partial t \\
&\partial V_3/\partial x_1 + \kappa_1 V_2 - \kappa_2 V_1 + (1+\gamma_{11})\Omega_2 - 2\gamma_{12}\Omega_1 = 2\partial \gamma_{13}/\partial t \\
&\partial \Omega_1/\partial x_1 + \kappa_2 \Omega_3 - \kappa_3 \Omega_2 = \partial \kappa_1/\partial t \\
&\partial \Omega_2/\partial x_1 + \kappa_3 \Omega_1 - \kappa_1 \Omega_3 = \partial \kappa_2/\partial t \\
&\partial \Omega_3/\partial x_1 + \kappa_1 \Omega_2 - \kappa_2 \Omega_1 = \partial \kappa_3/\partial t
\end{aligned}
\tag{1}
$$

where **F**, **M**, **V** and **Ω** are the vectors of sectional force, sectional moment, linear velocity and angular velocity, respectively. Furthermore, **P**, **H**, **γ** and **κ** are the vectors of sectional linear momenta, sectional angular momenta and generalized strain measures respectively. Here, the external force and moments (aerodynamic and distributed load) are denoted by **f** and **m** and can be written as

$$
\begin{aligned}
&\mathbf{f} = \mathbf{f}_{aero} + \mathbf{f}_{dis} \\
&\mathbf{m} = \mathbf{m}_{aero} + \mathbf{m}_{dis}
\end{aligned}
\tag{2}
$$

It must be noted that all these variables are described in the deformed reference frame [45].

The linear and angular momenta are related to the linear and angular velocities through the mass matrix as

$$\begin{bmatrix} P_1 \\ P_2 \\ P_3 \\ H_1 \\ H_2 \\ H_3 \end{bmatrix} = \begin{bmatrix} \mu & 0 & 0 & 0 & \mu x_3 & -\mu x_2 \\ 0 & \mu & 0 & -\mu x_3 & 0 & 0 \\ 0 & 0 & \mu & \mu x_2 & 0 & 0 \\ 0 & -\mu x_3 & \mu x_2 & i_2 + i_3 & 0 & 0 \\ \mu x_3 & 0 & 0 & 0 & i_2 & i_{23} \\ -\mu x_2 & 0 & 0 & 0 & i_{23} & i_3 \end{bmatrix} \begin{bmatrix} V_1 \\ V_2 \\ V_3 \\ \Omega_1 \\ \Omega_2 \\ \Omega_3 \end{bmatrix} \tag{3}$$

where μ is the beam mass per unit length, **x** is the vector of offsets between the centre of gravity and beam reference axis, and **i** is the vector of mass moment of inertia of the beam.

Furthermore, the internal force and moment can be obtained from the generalised strain measures using the cross-sectional stiffness matrix as

$$\begin{bmatrix} F_1 \\ F_2 \\ F_3 \\ M_1 \\ M_2 \\ M_3 \end{bmatrix} = \begin{bmatrix} S_{11} & S_{12} & S_{13} & S_{14} & S_{15} & S_{16} \\ S_{12} & S_{22} & S_{23} & S_{24} & S_{25} & S_{26} \\ S_{13} & S_{23} & S_{33} & S_{34} & S_{35} & S_{36} \\ S_{14} & S_{24} & S_{34} & S_{44} & S_{45} & S_{46} \\ S_{15} & S_{25} & S_{35} & S_{45} & S_{55} & S_{56} \\ S_{16} & S_{26} & S_{36} & S_{46} & S_{56} & S_{66} \end{bmatrix} \begin{bmatrix} \gamma_{11} \\ 2\gamma_{12} \\ 2\gamma_{13} \\ \kappa_1 \\ \kappa_2 \\ \kappa_3 \end{bmatrix} \tag{4}$$

where **S** is the matrix including the cross-sectional stiffness values of the beam. As stressed earlier, in this study the focus is on the three elastic couplings that might appear in composite beams. These are S_{14}, the extension-twist coupling, S_{45}, flap-twist coupling and S_{46}, lag-twist coupling. It must be noted that in what follows, it will be shown that these three couplings are the most effective couplings that can influence the aeroelastic stability of composite wings.

To simulate the aerodynamic loads of the wing, the unsteady incompressible finite-state Peter's formulation is implemented here in the form of intrinsic variables [46]. Therefore, the aerodynamic forces and moments in the aerodynamic reference frame at the quarter chord can be written as

$$\begin{bmatrix} f_{1_{aero}} \\ f_{2_{aero}} \\ f_{3_{aero}} \end{bmatrix} = [C_a] \begin{bmatrix} F_{a_1} \\ F_{a_2} \\ F_{a_3} \end{bmatrix}$$
$$\begin{bmatrix} m_{1_{aero}} \\ m_{2_{aero}} \\ m_{3_{aero}} \end{bmatrix} = [C_a] \begin{bmatrix} M_{a_1} + y_{ac} F_{a_3} \\ M_{a_2} \\ M_{a_3} - y_{ac} F_{a_1} \end{bmatrix} \tag{5}$$

where C_a is a transformation matrix from aerodynamic reference frame to the beam reference frame, and y_{ac} is the offset between the aerodynamic centre (quarter chord) and the beam reference axis. Then, the unsteady aerodynamic forces and moments in the aerodynamic reference frame can be written as

$$F_{a_1} = 0 \tag{6}$$

$$F_{a_2} = \rho b\left(-C_{l_0}V_T V_{a_3} + C_{l_\alpha}\left(V_{a_3} + \lambda_0\right)^2 - C_{d_0}V_T V_{a_2}\right)$$

$$F_{a_3} = \rho b\left(C_{l_0}V_T V_{a_2} - C_{l_\alpha}\dot{V}_{a_3} b/2 - C_{l_\alpha}V_{a_2}\left(V_{a_3} + \lambda_0 - \Omega_{a_1} b/2\right) - C_{d_0}V_T V_{a_3}\right)$$

$$M_{a_1} = 2\rho b^2\left(C_{m_0}V_T^2 - C_{m_\alpha}V_T V_{a_3} - C_{l_\alpha}V_{a_2}\Omega_{a_1} b/8 - C_{l_\alpha}\left(b^2/32\dot{\Omega}_{a_1} - b/8\dot{V}_{a_3}\right)\right)$$

$$M_{a_2} = 0$$

$$M_{a_3} = 0$$

where ρ and b are the air density and semi-chord of the wing, respectively. Furthermore, C_{l_0}, C_{l_α}, C_{d_0}, C_{m_0}, and C_{m_α} are the lift and pitching moment coefficients of the wing airfoil. Also, the subscript ($_a$) defines the variables in the aerodynamic reference frame, and V_T is the total velocity in the aerodynamic frame which is

$$V_T = \sqrt{V_{a_2}^2 + V_{a_3}^2} \tag{7}$$

The inflow, λ_0, appeared in Eq. 5 can be obtained using

$$\lambda_0 = \frac{1}{2}\{B\}^T\{\lambda\} \tag{8}$$

where $\{\lambda\}$ is a vector of inflow states that can be obtained using the following differential equations thus

$$[A]\{\dot{\lambda}\} + \left(\frac{V_T^n}{B^n}\right)\{\lambda\} = \left(-\dot{V}_{a_3} + \frac{b}{2}\dot{\Omega}_{a_3}\right)\{C\} \tag{9}$$

and $[A]$, $\{B\}$, and $\{C\}$ are pre-defined matrices/vectors defined as

$$[A] = [D] + \{d\}\{B\}^T + \{C\}\{d\}^T + \frac{1}{2}\{C\}\{B\}^T$$

$$B_n = \begin{cases} (-1)^{n-1}\dfrac{(N+n-1)!}{(N-n-1)!}\dfrac{1}{(n!)^2} & n \neq N \\ (-1)^{n-1} & n = N \end{cases}$$

$$C_n = \frac{2}{n}$$

$$d_n = \begin{cases} \frac{1}{2} & (n \neq 1) \\ 0 & (n = 1) \end{cases} \tag{10}$$

$$D_{nm} = \begin{cases} \dfrac{1}{2n} & (n = m+1) \\ -\dfrac{1}{2n} & (n = m-1) \\ 0 & (n \neq m \pm 1) \end{cases}$$

The wing modelled here as a cantilevered beam, and therefore the following boundary conditions will close the governing equations

$$\begin{bmatrix} F_1(L,t) \\ F_2(L,t) \\ F_3(L,t) \end{bmatrix} = \begin{bmatrix} 0 \\ 0 \\ 0 \end{bmatrix} , \begin{bmatrix} M_1(L,t) \\ M_2(L,t) \\ M_3(L,t) \end{bmatrix} = \begin{bmatrix} 0 \\ 0 \\ 0 \end{bmatrix} , \begin{bmatrix} V_1(0,t) \\ V_2(0,t) \\ V_3(0,t) \end{bmatrix} = \begin{bmatrix} 0 \\ U_\infty \\ 0 \end{bmatrix} , \begin{bmatrix} \Omega_1(0,t) \\ \Omega_2(0,t) \\ \Omega_3(0,t) \end{bmatrix} = \begin{bmatrix} 0 \\ 0 \\ 0 \end{bmatrix} \quad (11)$$

where U_∞ is the free-stream velocity of the wing.

The final aeroelastic equations can be obtained by combining Eqs. 1 and 6 which are then discretized here using a space-time scheme [45]. The aeroelastic stability of the system is sought by checking the eigenvalues of the linearized equations. To do this, first the time derivative variables are removed from the nonlinear aeroelastic equations, and the steady-state condition of the system is obtained using Newton-Raphson scheme. Then, the equations are linearized about this steady-state condition and the eigenvalues of the linearized system are determined.

Validation

An aeroelastic tool has been developed to capture the aeroelasticity of general composite high aspect ratio wings based on the above modelling approach. To validate the developed aeroelastic tool, in the first step, the flutter speed and frequency of an isotropic HALE wing with the properties presented in Table 1 are compared with those obtained by Patil et al. [6] for unloaded condition and by Patil and Hodges [4] for loaded cases. Table 2 and Figure 3 show the comparison of the results, and a very good agreement is observed. It is noted that for the loaded cases, a vertical distributed load along the span of the wing is considered. The results show that the stability of the wing is sensitive to the distributed load which is an effect of the structural nonlinearity available in the system.

Table 1: The HALE wing data ([6])

Parameter	Value
Half span (m)	16
Chord (m)	1
Mass per unit length (kg/m)	0.75
Moment of Inertia (50% chord) (kg.m)	0.1
Centre of gravity	50% of chord
Spanwise elastic axis	50% of chord
S_{44} (N.m^2)	1.0×10^4
S_{55} (N.m^2)	2.0×10^4
S_{66} (N.m^2)	4.0×10^6

c_{l_α}	2π

Table 2: Aeroelastic stability of the HALE wing (unloaded)

	Present	**Patil et al. [6]**
Flutter speed (m/s)	32.2	32.21
Flutter frequency (rad/s)	22.57	22.61

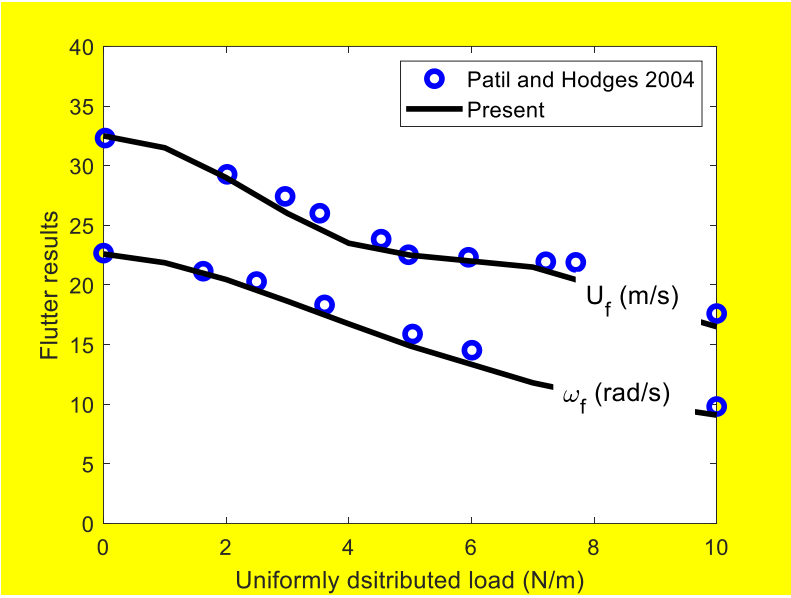

Figure 3: The effect of uniformly distributed load on the aeroelastic stability of the HALE wing (loaded)

Next, the free vibration of a composite rectangular solid section beam with properties presented in Table 3 is considered. Table 4 compares the first four natural frequencies of the beam with those obtained by Hodges et al. [47]. A very satisfactory agreement has been achieved, revealing that the developed methodology works fine for the composite beam applications. It is noted that in [47], the geometrically exact mixed beam formulation was used, and the results were obtained using finite element method.

Table 3: Solid rectangular composite beam properties ([47])

Parameter	**Value**
l (m)	0.56032

μ (kg/m)	7.3774×10^{-2}
i_{22} (kg.m)	1.4604×10^{-8}
i_{33} (kg.m)	5.5425×10^{-6}
S_{11} (N)	3.6102×10^{6}
S_{12} (N)	-2.0706×10^{5}
S_{22} (N)	4.1675×10^{5}
S_{33} (N)	3.0239×10^{4}
S_{44} (N.m^2)	3.5844×10^{-1}
S_{45} (N.m^2)	9.8951×10^{-2}
S_{55} (N.m^2)	5.3149×10^{-1}
S_{66} (N.m^2)	2.6342×10^{2}

Table 4: Comparison of natural frequencies of a thin composite beam with $[45,0]_{3s}$

Mode	**Present**	**Hodges et al. [47]**
1B (Hz)	4.664	4.66
2B (Hz)	29.604	29.6
3B (Hz)	84.90	84.89
1T (Hz)	113.43	113.43

Aeroelastic stability

From here on, a composite high aspect ratio wing with the properties listed in Table 5 which has a rectangular box spar is considered. This composite spar-box is designed so that the flutter speed and frequency values at ply angle of $\theta = 0^o$ be close to the HARW wing flutter speed and frequency values presented in Table 2. The dimensions and material properties of the designed baseline spar-box are summarised in Table 5. Table 6 also presents the cross-sectional stiffness values of the spar-box at $\theta = 0^o$. It must be noted that here, the mass per unit length and the moment of inertia of the baseline wing is assumed to be the same as the HALE wing, and hence the change in the stiffness matrix (**S**) is the primary focus of this study.

Table 5: Geometrical and material properties of the composite spar box

Parameter	Value
w_s (mm)	580.0
h_s (mm)	42.0
t_s (mm)	0.75
Number of layers	6
Thickness of each layer (mm)	0.125
E_1 (GPa)	142
$E_2 = E_3$ (GPa)	9.81
G_{23} (GPa)	3.77
$G_{12} = G_{13}$ (GPa)	6.0
ν_{23}	0.34
$\nu_{12} = \nu_{13}$	0.3

Table 6: Cross-sectional stiffness of the baseline composite wing ($\theta = 0^o$)

Parameter	Value
S_{11} (N)	1.32806×10^8
S_{22} (N)	4.6165×10^6
S_{33} (N)	7.3667×10^4
S_{44} (N.m^2)	8.9488×10^3
S_{55} (N.m^2)	5.7921×10^4
S_{66} (N.m^2)	4.2445×10^6

Table 7 compares the first five natural frequencies of the designed composite baseline wing with the HALE wing reported by Patil et al [10]. It is clear that the frequencies are close to the HALE wing with the properties presented in Table 2.

Table 7: Natural frequencies of the baseline wing ($\theta = 0^o$)

Mode	Frequency (rad/s)	Frequency (rad/s) [10]
1st flap (out of plane)	3.8	2.25

2nd flap (out of plane)	23.65	14.61
3rd flap (out of plane)	66.12	44.01
1st torsion	29.43	31.15
1st lag (in plane)	32.47	31.74

The flutter speed and frequency of the baseline composite wing are compared with those obtained for HALE wing and reported in Table 8. Both the flutter speed and frequency of the designed baseline wing are close to those of the HALE wing. Furthermore, Figure 4 and 5 show the variation of the aeroelastic frequencies and damping of the baseline composite wing with respect to the free-stream velocity at ply angle $\theta = 0^o$. It is clear that the first flap and first torsion frequencies are dominant in the flutter mechanism of the baseline wing at this specific ply angle.

Table 8: Comparison of the flutter speed and frequency of the designed baseline composite wing with the HALE wing

	Present	**HALE**
Flutter speed (m/s)	32.5	32.2
Flutter frequency (rad/s)	20.42	22.57

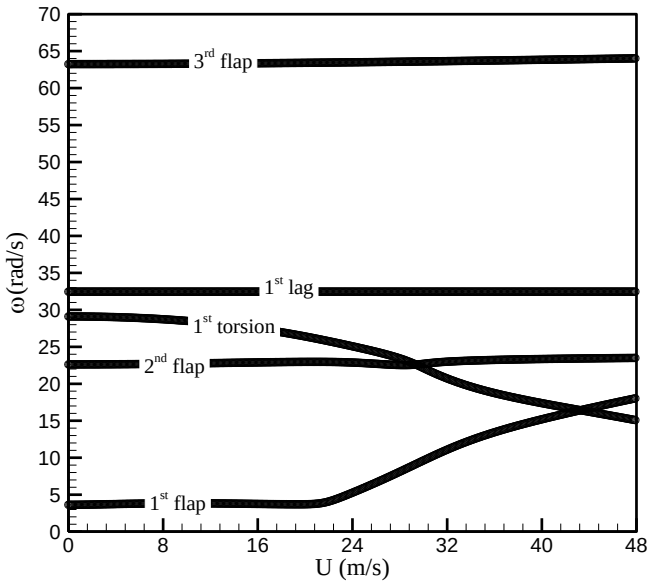

Figure 4: The aeroelastic frequencies of the baseline composite wing ($\theta = 0^o$)

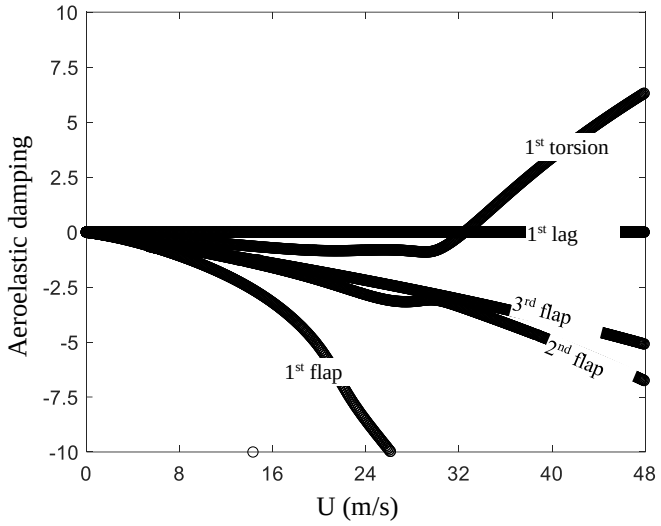

Figure 5: The aeroelastic damping of the baseline composite wing ($\theta = 0^o$)

In what follows, the aeroelastic stability of various composite wings with different layups are studies. Three various layups are considered and summarised in Table 9. The first case is a representative of an anti-symmetric layup where the extension-twist coupling is dominant. The second and third cases are symmetric layups where the lag-twist and flap-twist couplings are dominant respectively.

Table 9: The three composite layup cases

	Top wall	Bottom wall	Left wall	Right wall
Case 1(E-T)	$[\theta]_6$	$[-\theta]_6$	$[\theta]_6$	$[-\theta]_6$
Case 2 (L-T)	$[\theta/-\theta]_3$	$[\theta/-\theta]_3$	$[\theta]_6$	$[\theta]_6$
Case 3 (F-T)	$[\theta]_6$	$[\theta]_6$	$[\theta/-\theta]_3$	$[\theta/-\theta]_3$

Firstly, the variation of composite wing frequencies for different ply angles are shown in Figures 6-8. In all three layup cases, the first and second flap modes reduce when the ply angle increases. For the first layup, as shown in Figure 6, the first lag and third flap modes also decrease with the increase of ply angle, while the first torsion mode first increases until $\theta = 45^o$, and then decreases. The same pattern happens for the second case, as shown in Figure 7, except that in this case, the lag and torsion modes veer away at $\theta = 5^o$. This effect is mostly is due to the lag-twist coupling that appears at this layup configuration. Moreover, for the third layup (Figure 8), the mode veering between torsion and third flap modes happens at around $\theta = 15^o$ due to the flap-twist coupling.

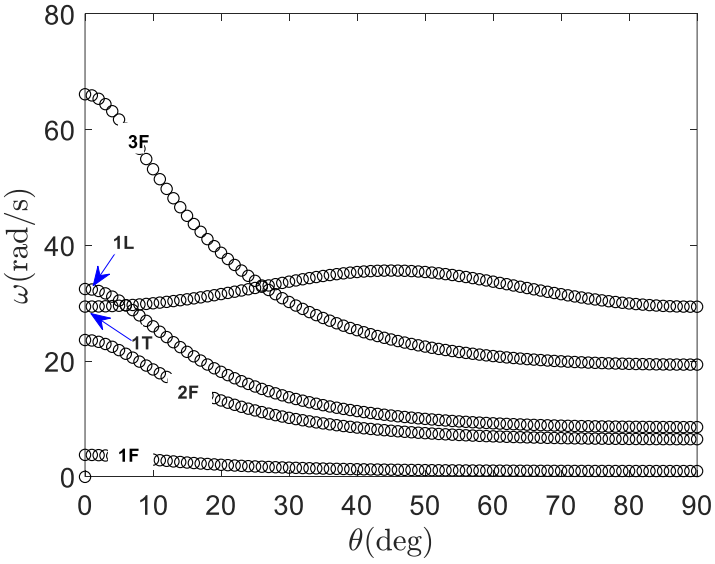

Figure 6: The effect of ply angle on the wing frequencies for case 1

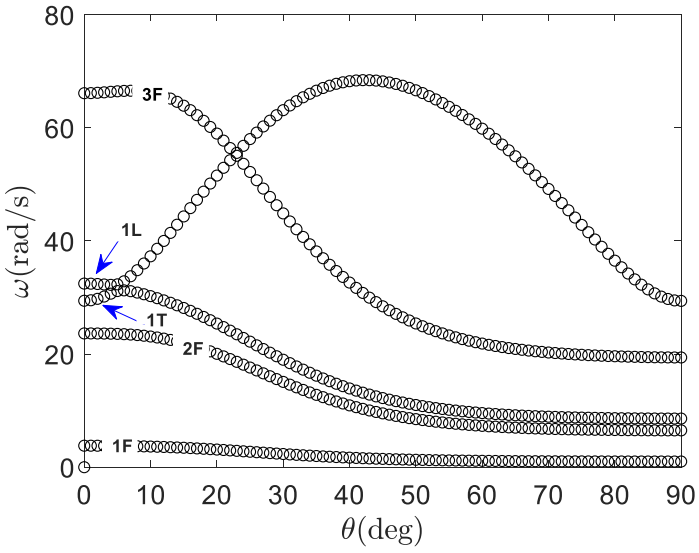

Figure 7: The effect of ply angle on the wing frequencies for case 2

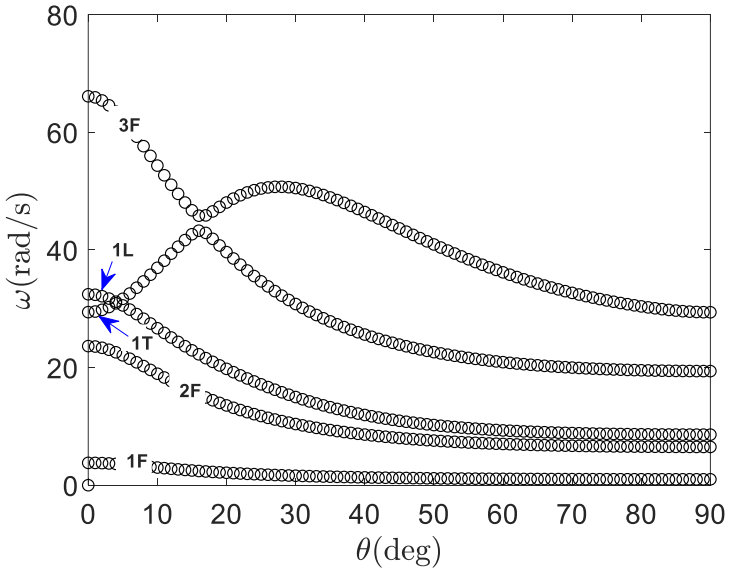

Figure 8: The effect of ply angle on the wing frequencies for case 3

Figure 9 shows the variation of normalized flutter speed and frequency of the first layup case where the extension-twist coupling is dominant. The trends of changes of flutter speed and frequency for this composite case are almost similar. It is noted that from here on, all the variables are nondimensionalised with respect to the values obtained at $\theta = 0^o$ (listed in Table 8). For this layup case, the results are symmetrical with respect to the ply angle θ, and hence the sign of the ply angle doesn't affect the results. The flutter speed initially decreases and then increases to reach the highest value at around $\theta = 45^o$, and then decreases again. It should be noted that the highest flutter frequency also happens at around $\theta = 45^o$. Furthermore, Figure 10 shows the aeroelastic frequency variation of the wing for various speeds for $\theta = 45^o$ at which the maximum flutter speed happens. As described in [27], the main reason of these changes in flutter speed and frequency is the interaction and couplings between modes as shown in the previous section.

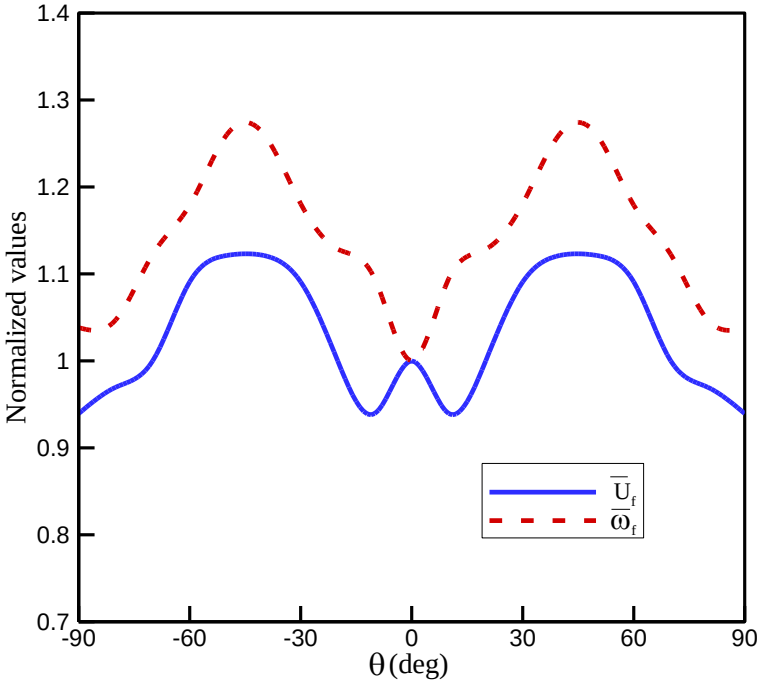

Figure 9: Aeroelastic instability of the baseline composite wing of case 1

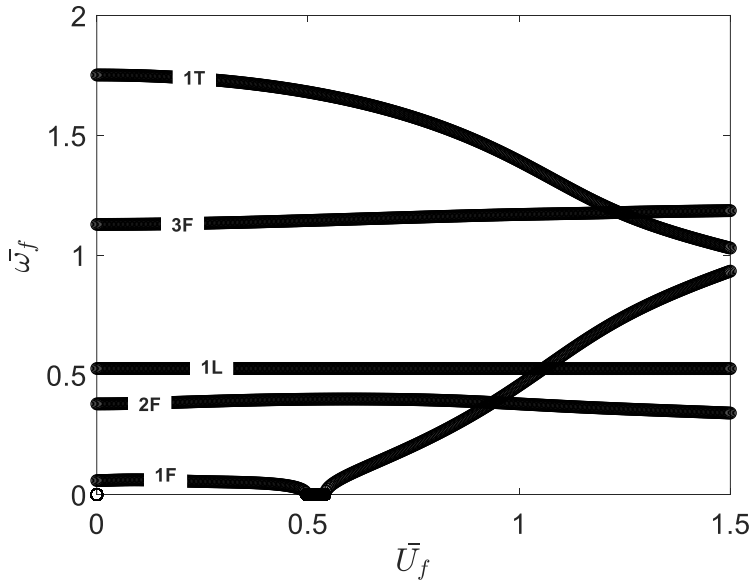

Figure 10: The aeroelastic frequencies of the baseline composite wing ($\theta = 45^o$)

Next, the aeroelastic instability of case 2 is considered and shown in Figure 11. It is clear that for this layup where the lag-twist coupling is dominant, the flutter speed and frequency values are symmetric with respect to the ply angle. Here, the flutter speed first increases and then decrease to reach the minimum value at around $\theta = 80^o$,

and then it increases at higher angles due to a change in modes contributing in the flutter mechanism. In this case, the maximum flutter speed appears at $\theta = 10^o$ which the aeroelastic frequencies at this ply angle is shown in Figure 12. In this case, first torsion and lag modes veer away at around $\bar{U}_f = 1$, and hence the flap and torsion modes coalescence.

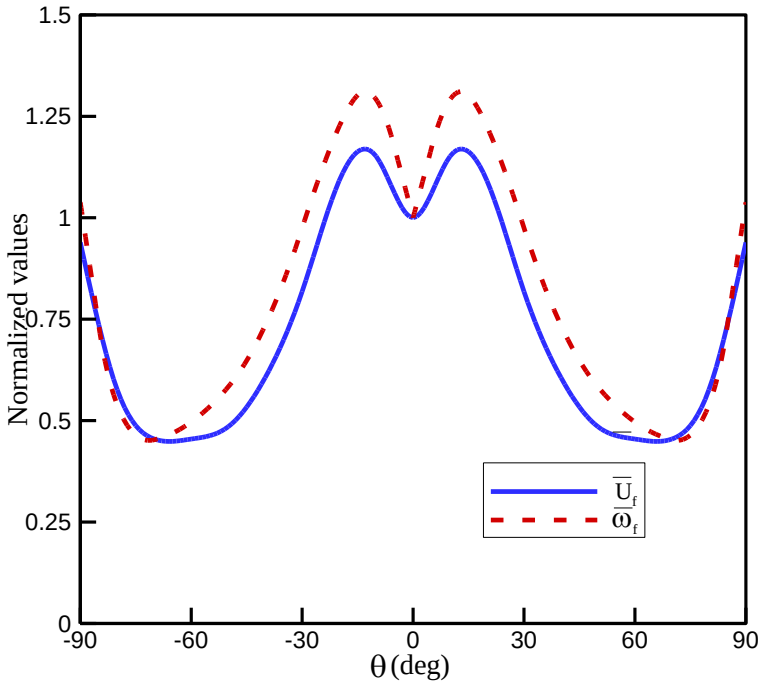

Figure 11: Aeroelastic instability of the baseline composite wing of case 2

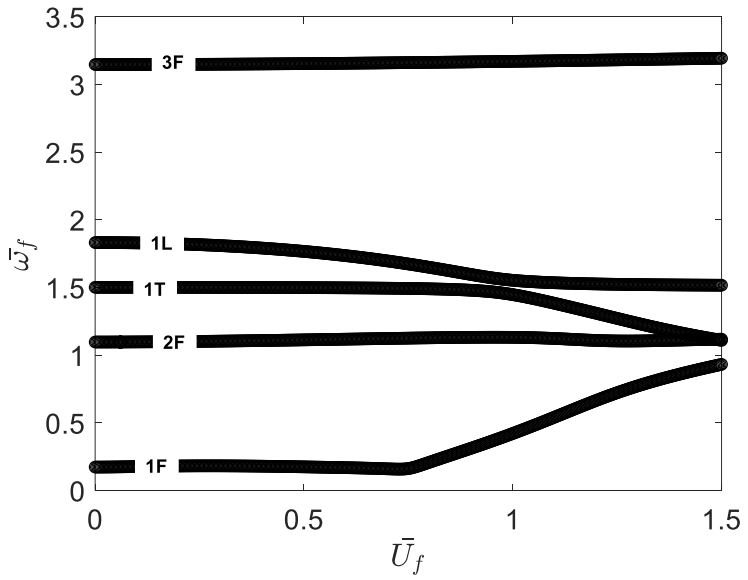

Figure 12: The aeroelastic frequencies of the baseline composite wing ($\theta = 10^o$)

Finally, the aeroelastic stability of the composite wing with case 3 configuration is considered and shown in Figure 13. For this case, the flap-twist coupling is dominant. For this case, the flutter speed first increases to reach the highest value at around $\theta = 25^o$, and then decreases. Also, Figure 14 shows the variation of aeroelastic frequencies of this layup for $\theta = 25^o$ clarifying that again here the flap and torsion modes are coupled to make the system unstable.

As the trend of the results are almost similar for the negative and positive ply angles for all layups, in what follows, only the positive ply angles are considered.

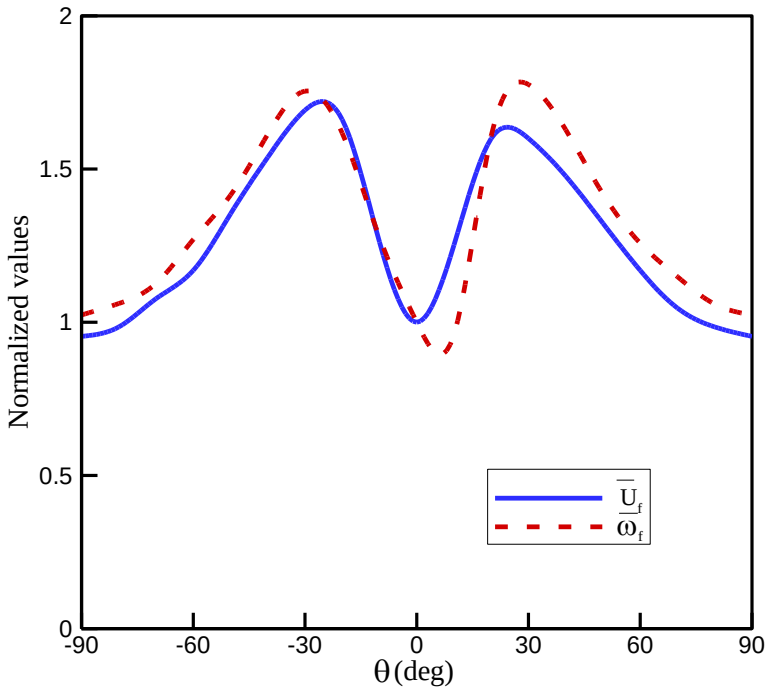

Figure 13: Aeroelastic instability of the baseline composite wing of case 3

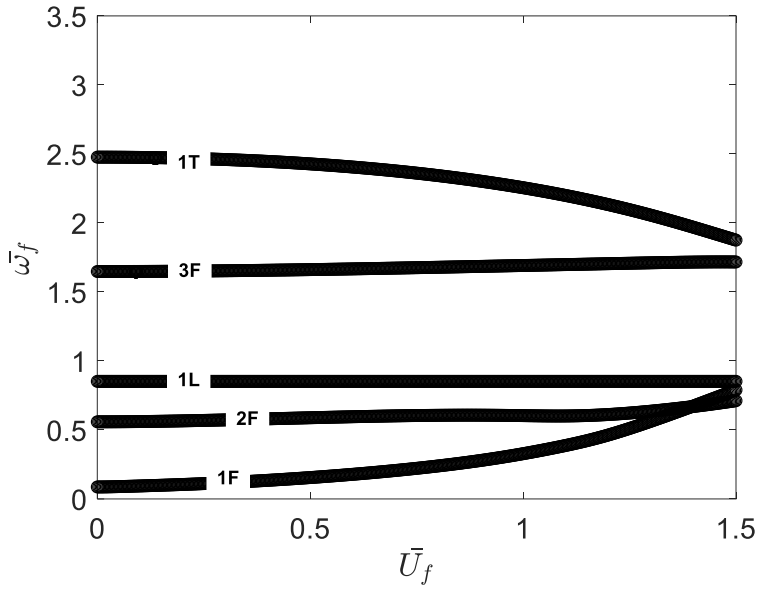

Figure 14: The aeroelastic frequencies of the baseline composite wing ($\theta = 25^o$)

Effect of uniformly distributed follower load on the aeroelastic stability

As it was shown before, due to structural nonlinearities, the stability of the wing is highly sensitive to the applied load. Therefore, in this section the aeroelastic stability of the composite wing under uniformly distributed vertical follower force (loaded condition) is investigated. In this study, it is assumed that the main load carrying part of the structure is the spar, which is a composite box. It should be noted that the spar-box is positioned in a way that the elastic axis of the wing always lies at the mid chord of the wing.

Figure 15 shows the flutter speed and frequency for case 1 configuration for three different load levels ($f_{3_{dis}}$) and ply angles. For this case, by increasing the load level, both flutter speed and frequency decreases for all ply angles. For the sake of consistency, the values are nondimensionalised with respect to the baseline values at zero ply angle. The main reason of flutter speed and frequency reduction for this layup is that by increasing the load level, the wing frequencies (specially the torsion) changes as shown in Figure 16. It is clear that at around θ=20º, the torsion and third flap modes veer away from each other, and hence the mode properties changes.

a)

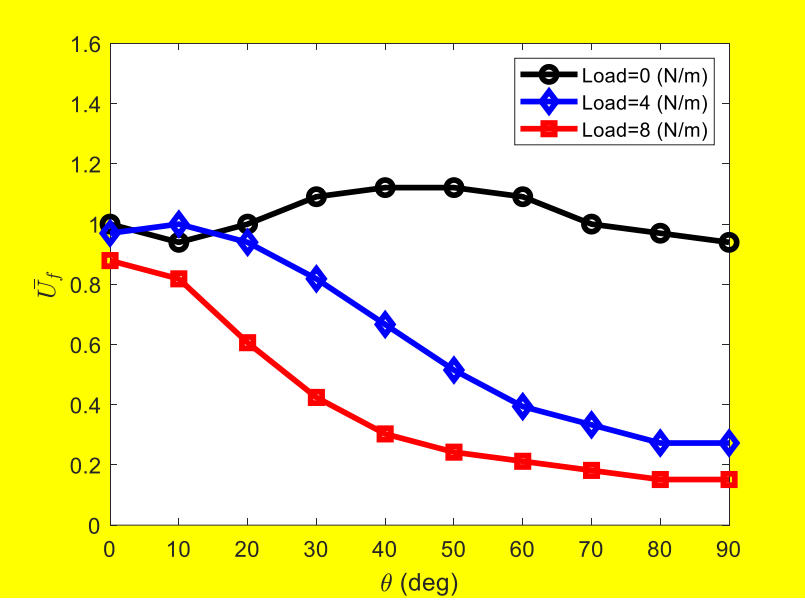

b)

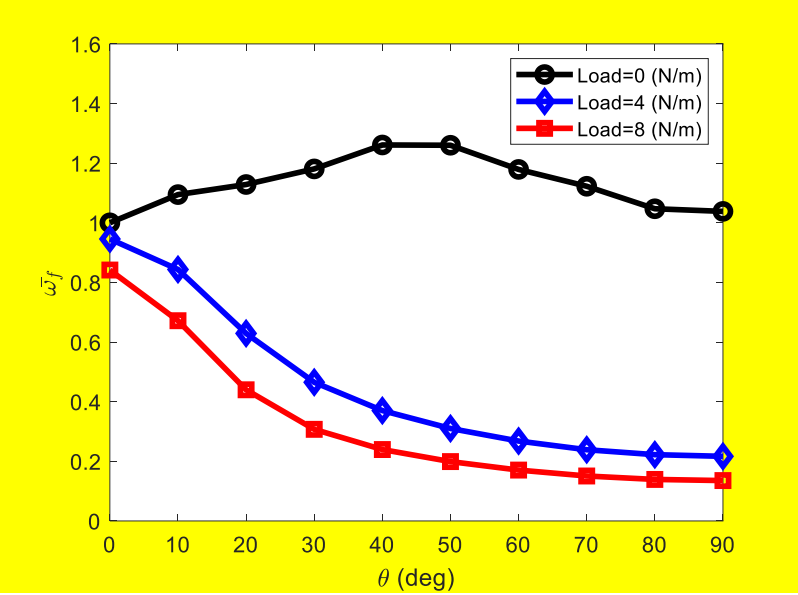

Figure 15: Effect of vertical load on the aeroelastic stability of the composite wing (case 1) a) flutter speed and b) frequency

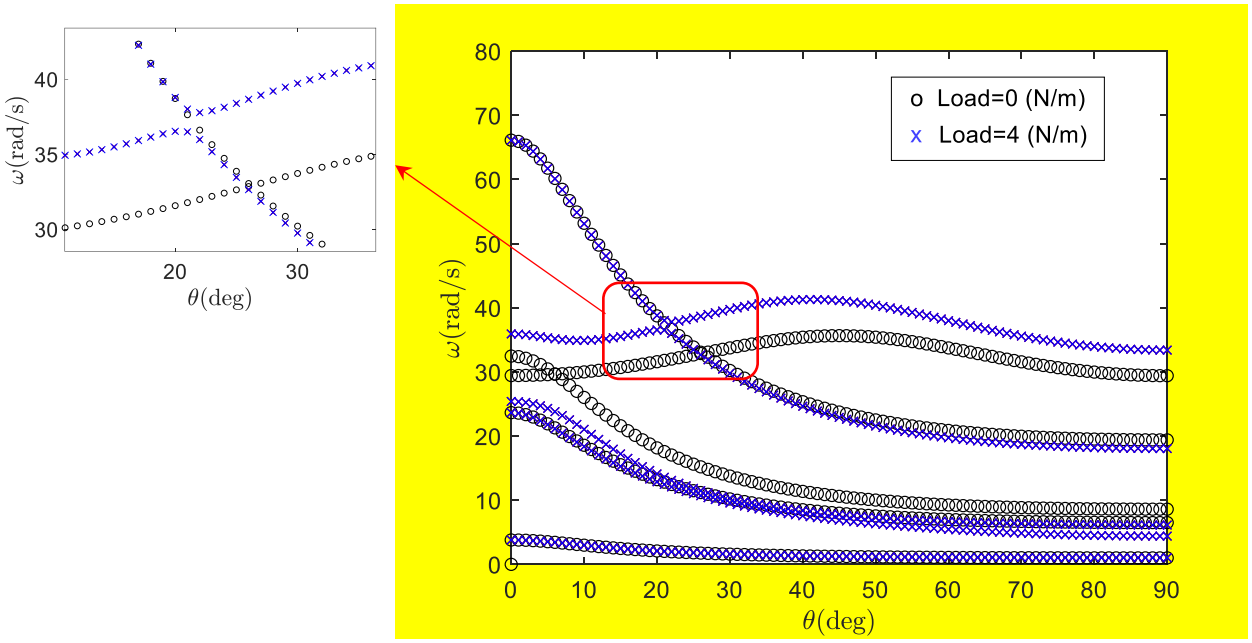

Figure 16: The effect of ply angle and vertical load on the wing frequencies for case 1

The effect of vertical load on the aeroelasticity of the case 2 with lag-twist coupling is determined and shown in Figure 17. In this case, again by increasing the load level, the flutter speed and frequency decrease, but the reduction percentage is smaller than case 1. As shown in Figure 18, the reason of this reduction is that the torsional mode frequency decreases when the load is applied, however the rate of reduction is lower than case 1.

a)

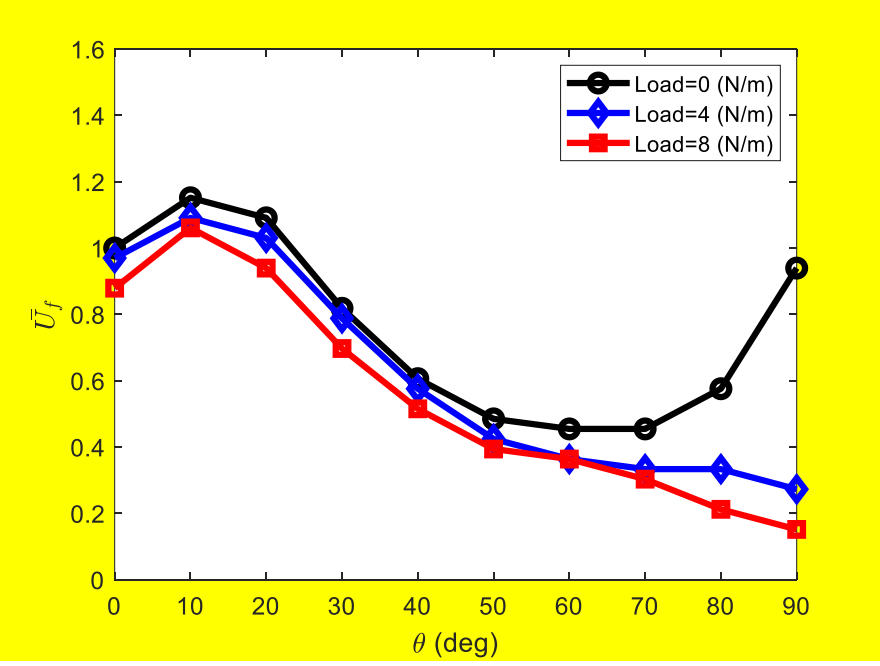

b)

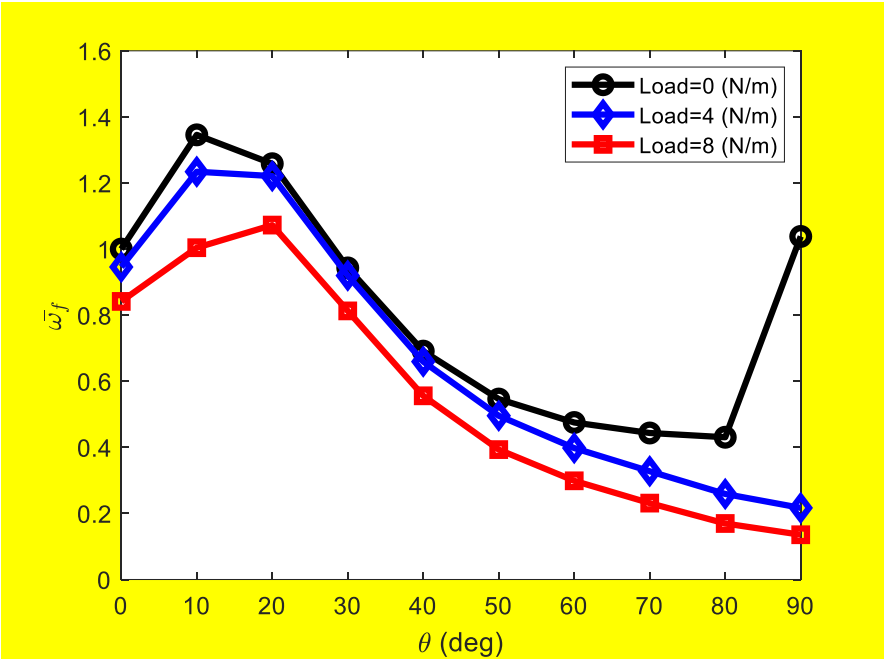

Figure 17: Effect of vertical load on the aeroelastic stability of the composite wing (case 2) a) flutter speed and b) frequency

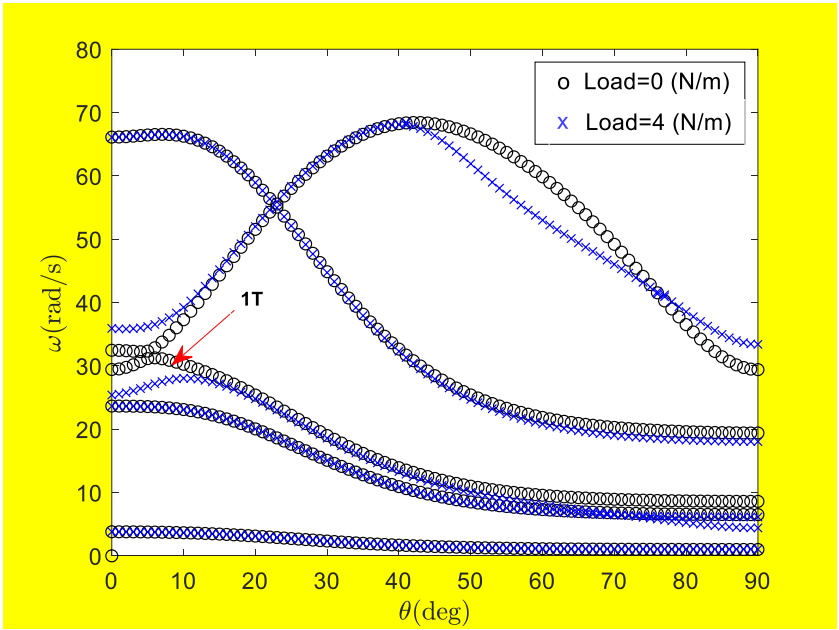

Figure 18: The effect of ply angle and vertical load on the wing frequencies for case 2

Figure 19 shows the variations of flutter speed and frequency of the case 3 layup with flap-twist coupling. The trend of this case is very interesting as the flutter speed and frequency do not change too much until θ=45°, and then decreases. By looking at the wing frequencies, shown in Figure 20, it is evident that the torsional mode is not so sensitive to the applied load and therefore, the flutter speed and frequency of the wing stays almost constant

until θ=45°. However, after this point, the modes that contribute in the flutter mechanism change, and this is the reason of a sudden reduction or jump seen in the flutter speed and frequency after this point.

a)

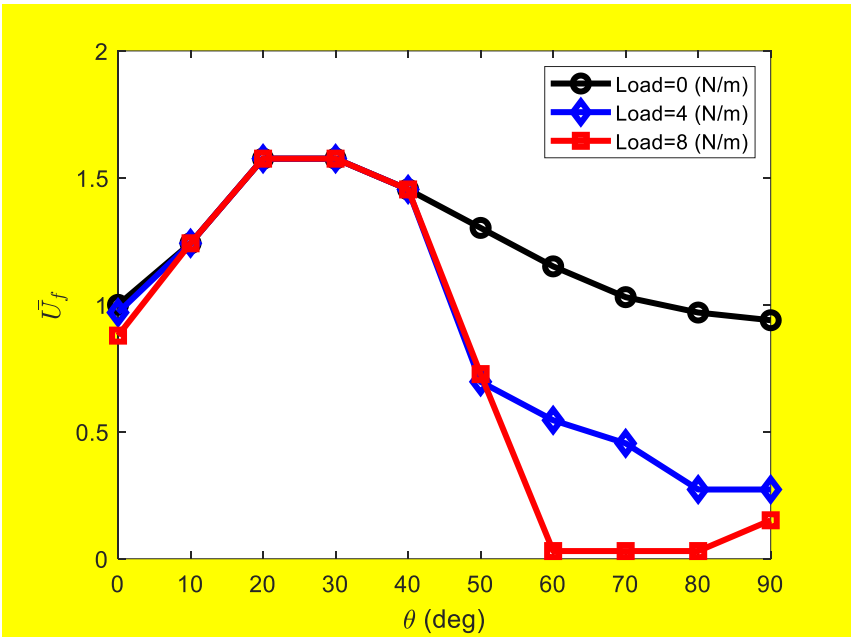

b)

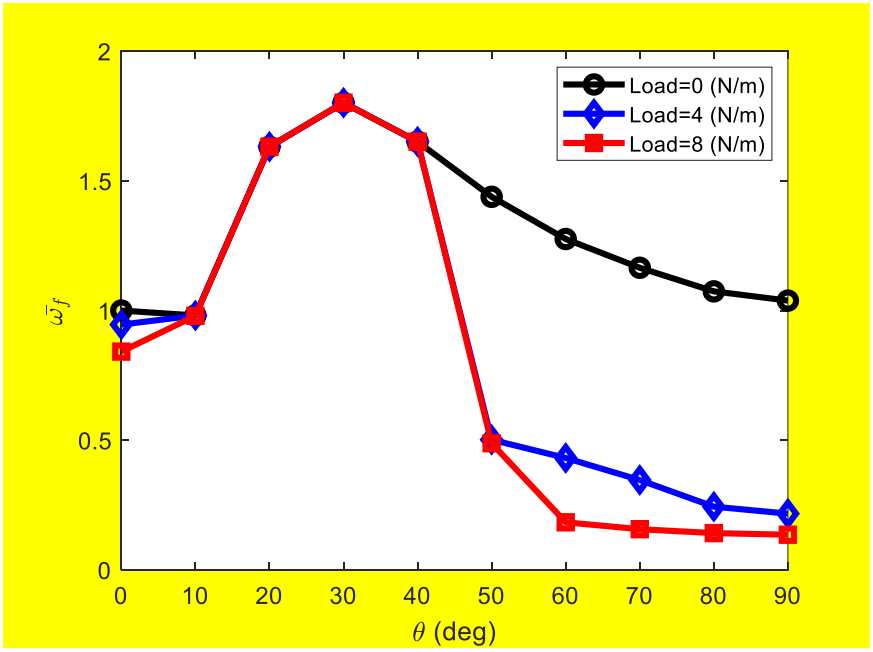

Figure 19: Effect of vertical load on the aeroelastic stability of the composite wing (case 3) a) flutter speed and b) frequency

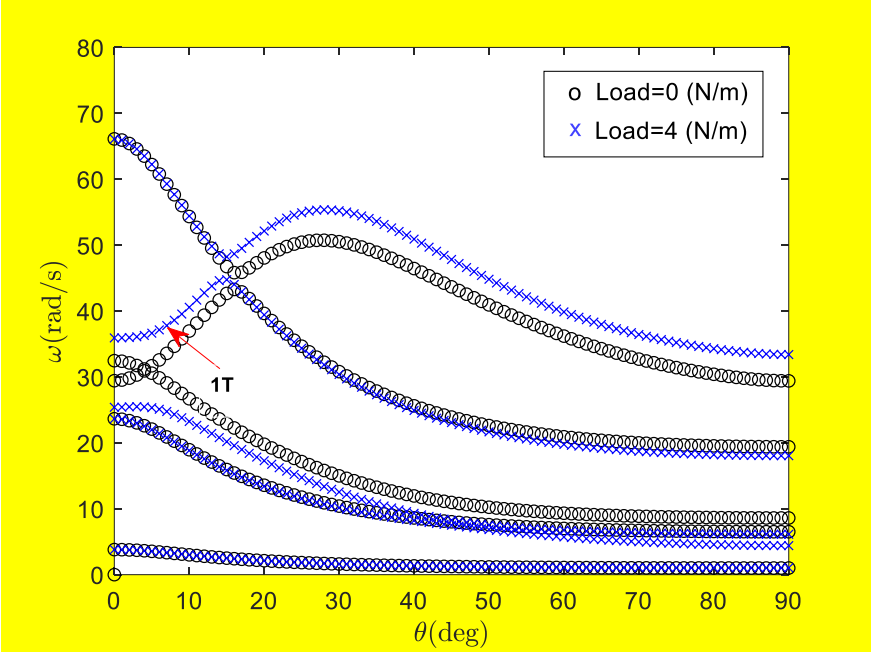

Figure 20: The effect of ply angle and vertical load on the wing frequencies for case 3

Uncertainty quantification

As the aeroelastic properties of the wing are very sensitive to the lamination parameters ([48]), it is important to understand the aeroelastic behaviour of the wing when there are uncertainties in the system due to manufacturing processes or degradations. In this section, the uncertainty quantification of high aspect ratio composite wing is investigated. The material properties of the composite wing are assumed to be independent uncertain random variables. This allows to easily assess changes in the aeroelastic instability when there are uncertain values in the material properties. Here, it is assumed that the material properties are randomly distributed with a defined coefficient of variation (COV) [39]. The COV is the ratio between the standard deviation to the samples' mean value. This coefficient normally can be determined either from experiments or simulations ([39]). Here, the randomness of the material properties is taken from ([36]) and presented in Table 10. Different COV values of the material properties are considered to replicate a more realistic case ([39]).

Table 10: Coefficient of variation of selected material properties

Material properties	Sample's mean value	Coefficient of variation (COV)
$\boldsymbol{E_1}$ **(GPa)**	142	7.0%
$\boldsymbol{E_2}$ **(GPa)**	9.81	4.0%
$\boldsymbol{G_{12}}$ **(GPa)**	6.0	11.0%

ν_{12}	0.34	4.0%

In the first step, it is necessary to determine how many samples in a Monte Carlo simulation is enough for the uncertainty analysis. To this aim, the convergence of the normalised standard deviation of the torsional, lag and flap stiffness values for various numbers of samples are determined and shown in Figure 21. It is apparent that by considering about 5000 samples, the standard deviation is converged. Therefore, in this study, 5000 samples are used for the Monte Carlo simulations, the same number of samples used by Murugan et al. [39].

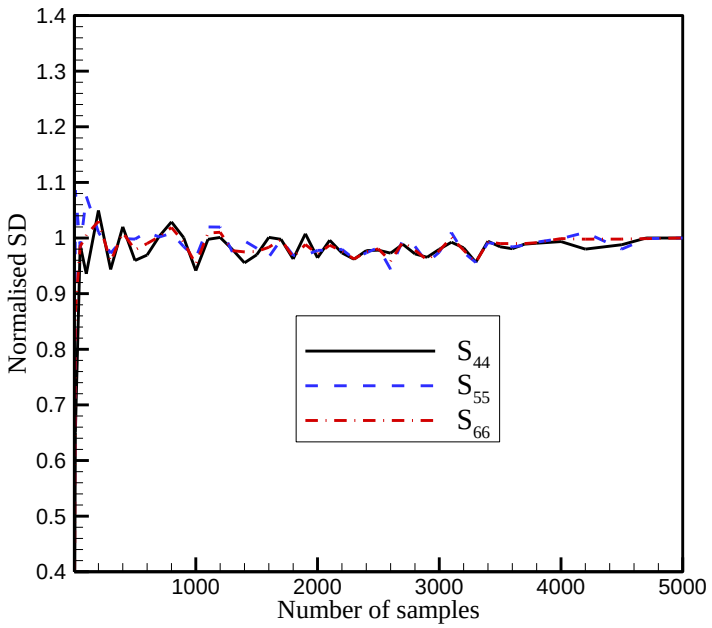

Figure 21: The normalised standard deviation convergence of stiffness values (S_{44}, S_{55}, S_{66})

A random sampling procedure is considered to produce the 5000 samples of the composite material properties. Figure 22 shows all the samples used for the Monte Carlo simulation for three out of four random parameters. Also, Figures 23-26 show the histogram of the probability of occurrence of random samples for the selected material properties.

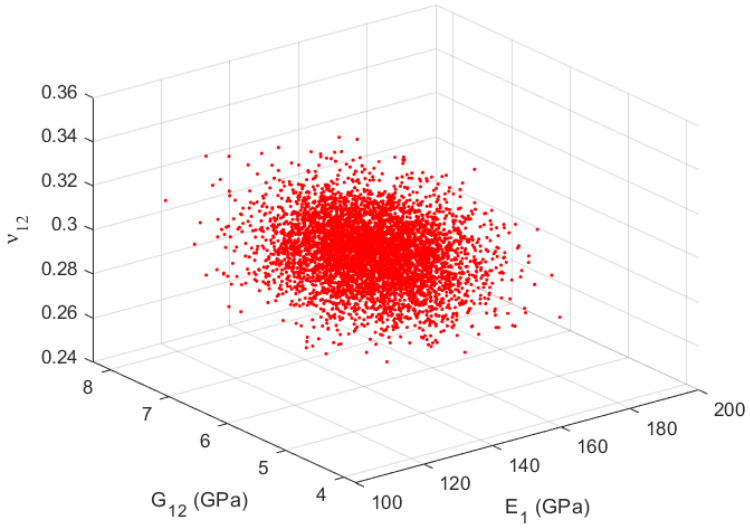

Figure 22: Monte Carlo samples of material properties of the composite wing

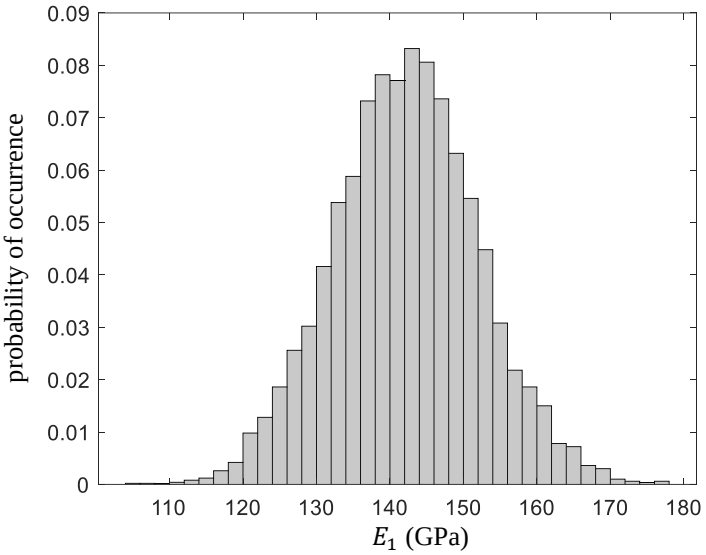

Figure 23: Histogram of the probability of occurrence of E_1

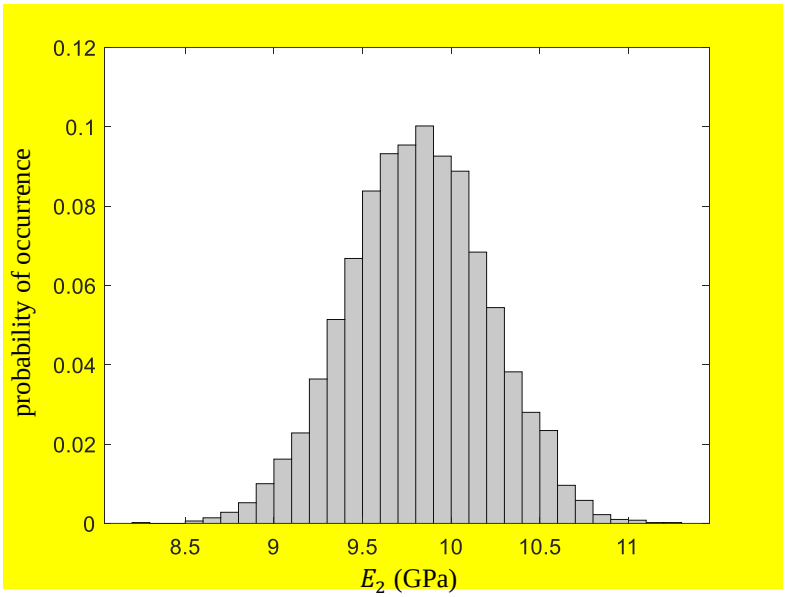

Figure 24: Histogram of the probability of occurrence of E_2

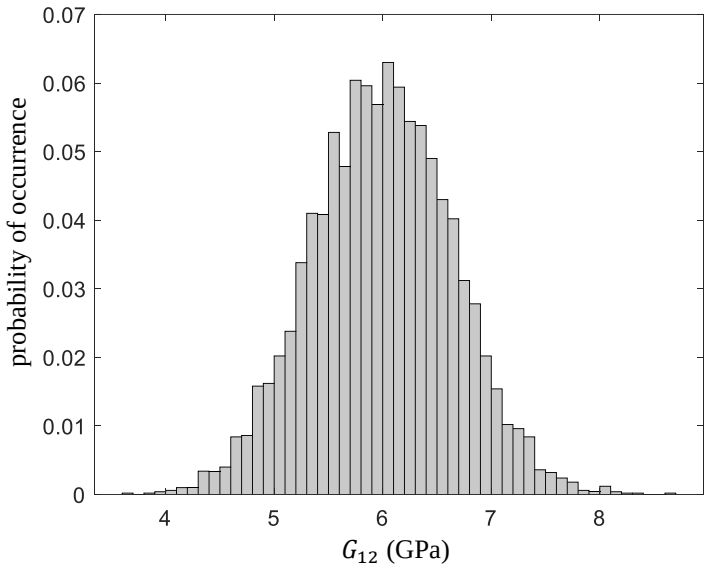

Figure 25: Histogram of the probability of occurrence of G_{12}

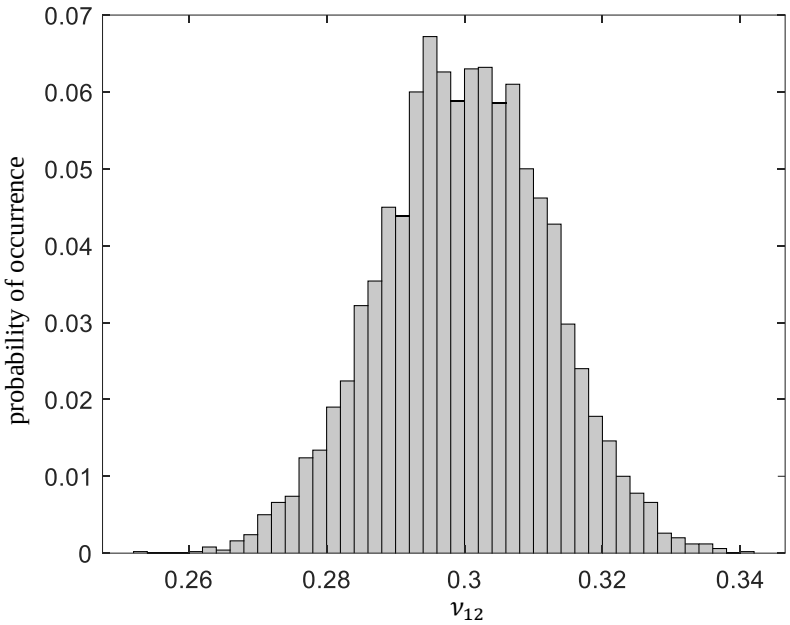

Figure 26: Histogram of the probability of occurrence of ν_{12}

The effect of randomness of the composite material properties on the aeroelastic stability of high aspect ratio wings is studied using the Monte Carlo simulation. To this aim, 5000 simulations, using the random materials prescribed in Table 10, are completed and the results are presented here.

In the first step, it is necessary to investigate how uncertainties in the material properties influence the elastic couplings of the composite wing. Figures 27-29 show the regions of variation of the nondimensional elastic couplings for various ply angles. It should be noted that the elastic coupling values are nondimensionalised with respect to the corresponding diagonal values in the stiffness matrix. The dashed line shows the elastic coupling of the baseline wing, and the shaded area covers the upper and lower variations of coupling for 5000 Monte Carlo simulations. It is clear that for all ply angles, there is a region of change when there are material uncertainties. However, the shaded domain is not symmetric around the baseline coupling values, and the ply angle at which the highest variation takes place differs for different elastic couplings. It should be noted that the highest variation of extension-twist, lag-twist, and flap-twist couplings take place in the regions between $60^o < \theta < 80^o$.

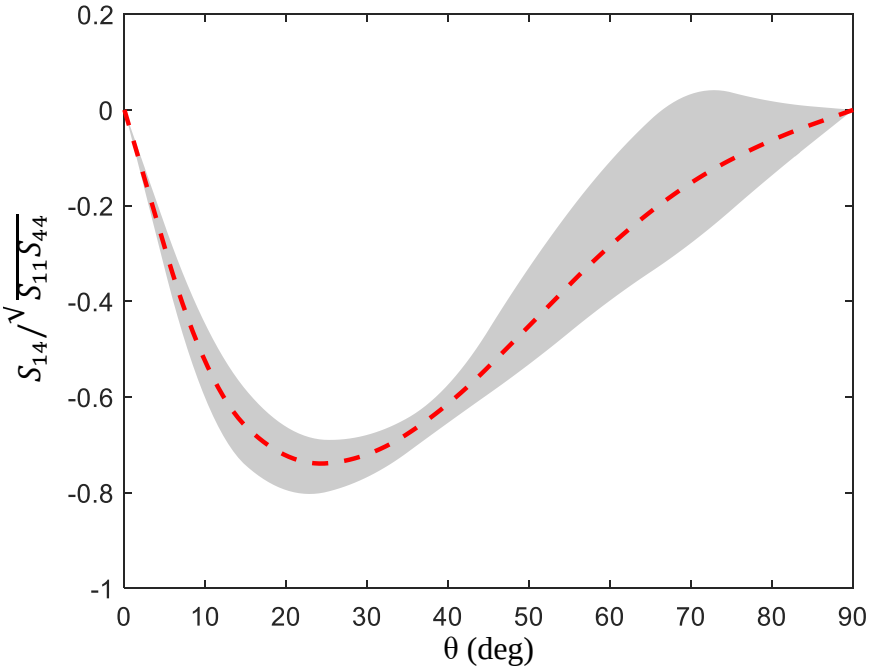

Figure 27: MCS of nondimensional extension-twist coupling of the baseline composite wing (case 1)

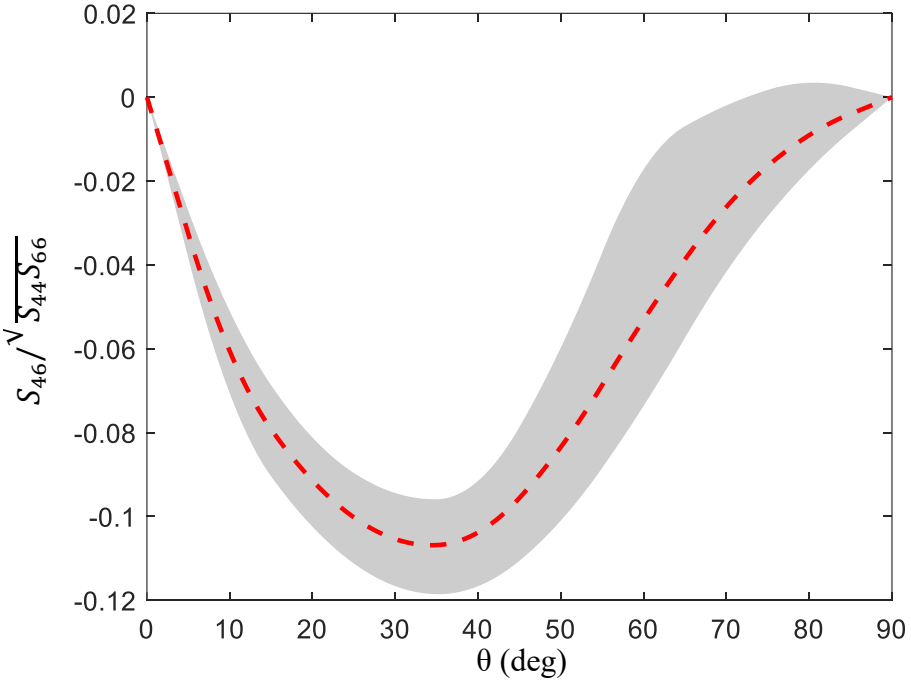

Figure 28: MCS of nondimensional lag-twist coupling of the baseline composite wing (case 2)

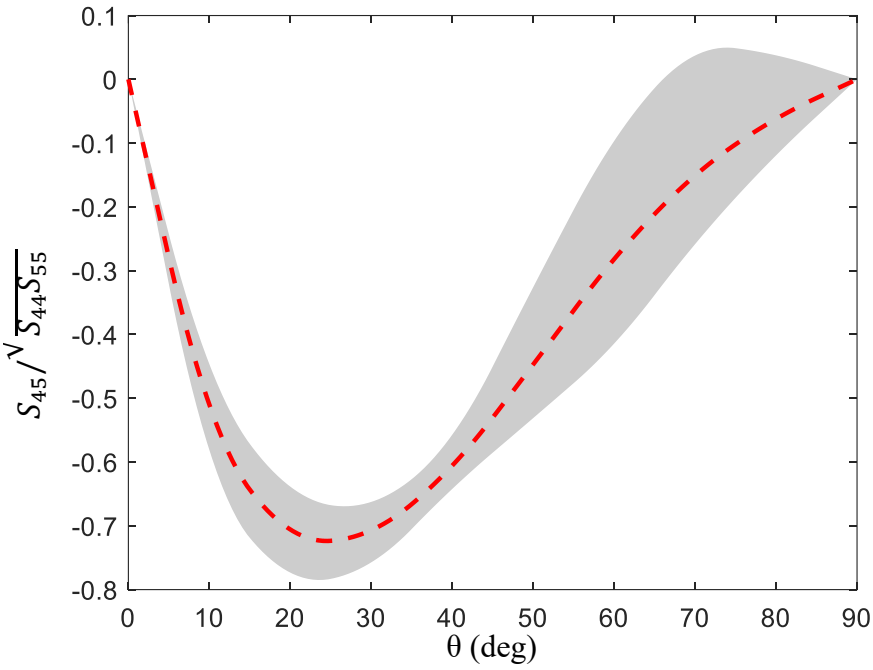

Figure 29: MCS of nondimensional flap-twist coupling of the baseline composite wing (case 3)

Figures 30-32 show the regions of variation of flutter speed and frequency for different layup cases (case 1 to 3). Again here, the dashed line represents the variation in flutter speed and frequency of the baseline wing for various ply angles. Furthermore, the shaded domain covers the results of 5000 Monte Carlo simulations. It should be noted that the flutter speed and frequency are nondimensionalized with respect to the values of baseline composite wing at zero ply angle. Figure 30 shows the variation of flutter speed and frequency of the wing with extension-twist coupling (case 1). For this layup, the maximum variation of flutter speed and frequency due to the uncertainty in material properties takes place at $\theta = 0^o$ and $\theta = 90^o$. Furthermore, the minimum variation happens at the middle of the plot and at $\theta = 45^o$. It must be noted that, the highest variation of flutter speed and frequency for this layup is about 25%. These results show that that aeroelastic stability of the wing is sensitive to any uncertainty that might occur in the material properties.

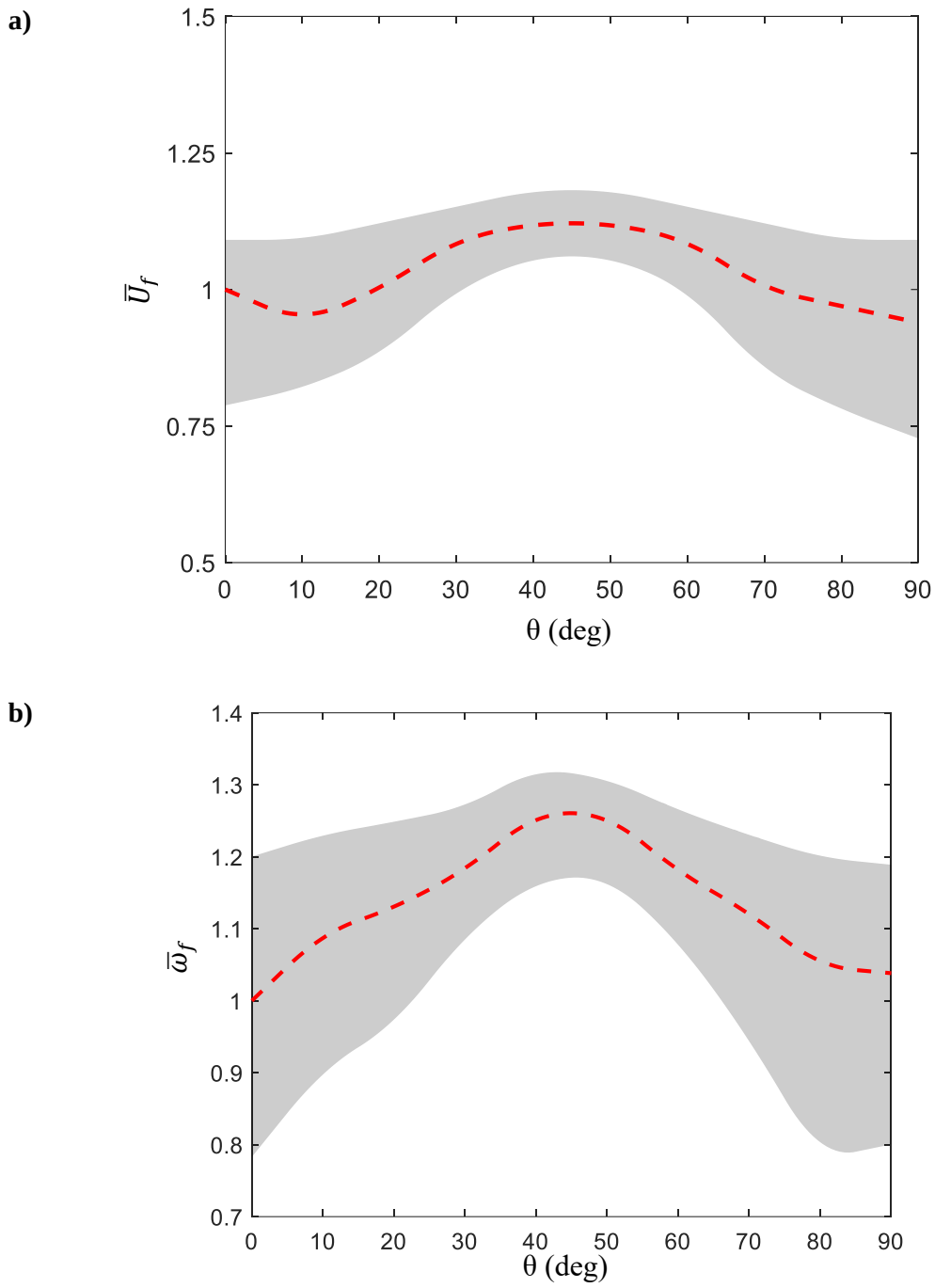

Figure 30: MCS of the baseline composite wing of case 1 for a) flutter speed b) flutter frequency

Figure 31 shows the nondimensional flutter speed and frequency variation of the second layup wing with lag-twist coupling. For this layup, the maximum variation in both flutter speed and frequency, due to uncertainty in material properties, happens around ply angle of $\theta = 80^o$. The maximum amount of variation for flutter speed is about 60% and for flutter frequency is almost 85%. This result shows that this layup configuration (case 2) is more sensitive to the variations in the material properties than the previous case (case 1).

a)

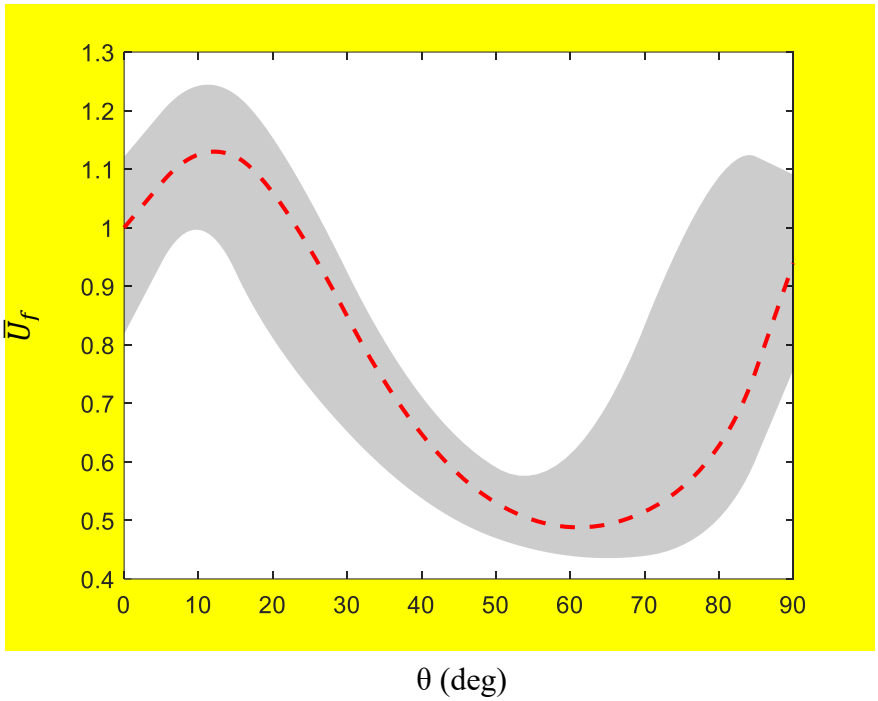

b)

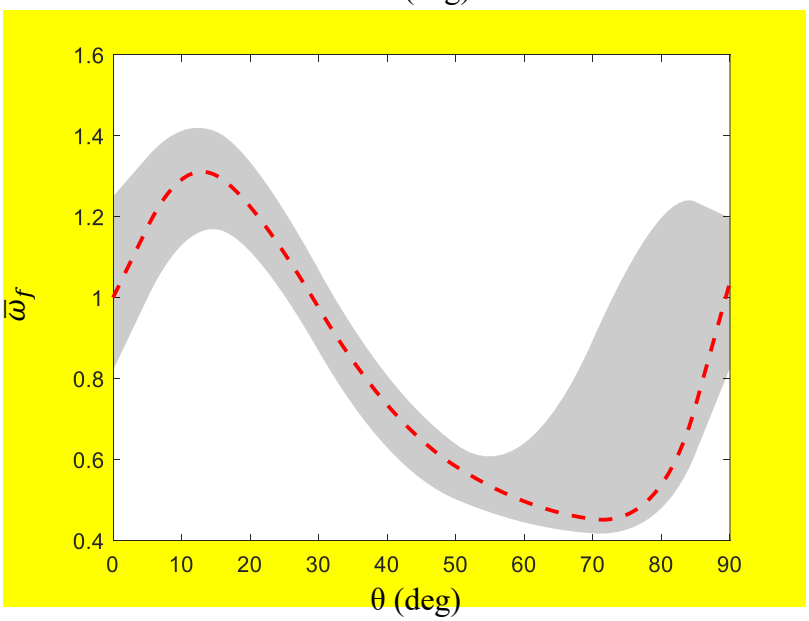

Figure 31: MCS of the baseline composite wing of case 2 for a) flutter speed b) flutter frequency

Finally, the effect of material uncertainties on the flutter speed and frequency of the layup with flap-twist coupling, case 3, are determined and shown in Figure 32. For this case, the maximum variation in flutter speed is about 20% and happens at ply angle of $\theta = 90^o$. Furthermore, the highest variation in flutter frequency happens at ply angles of $\theta = 0^o$ and $\theta = 90^o$ and the maximum change is about 20%. This behaviour shows that with the flap-twist coupling in the lamination, the aeroelastic instability is less sensitive to the uncertainty of material properties than the lag-twist coupling layup. Therefore, the analysis carried out here highlights that the uncertainty of aeroelastic behaviour of the composite wings depend on the type of lamination and elastic coupling exist in the layup.

a)

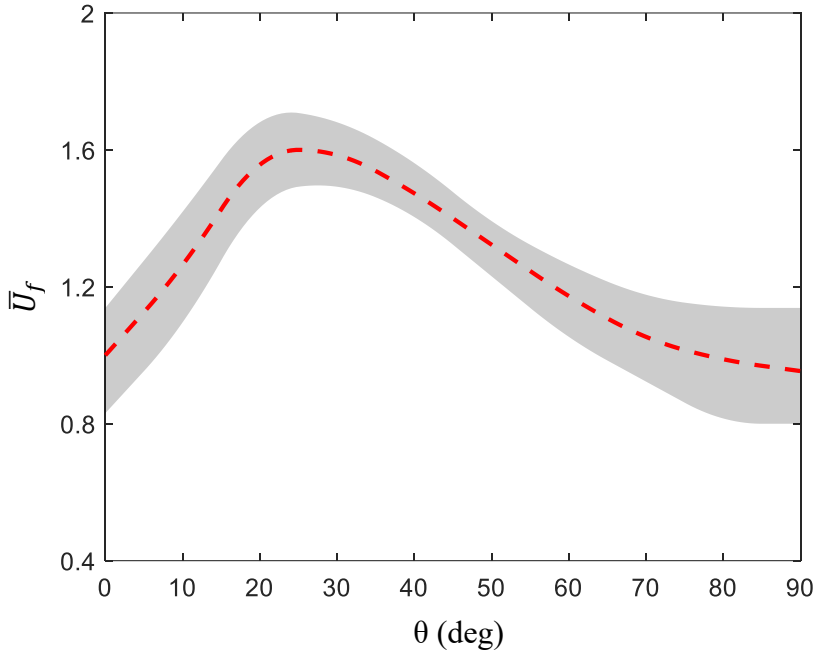

b)

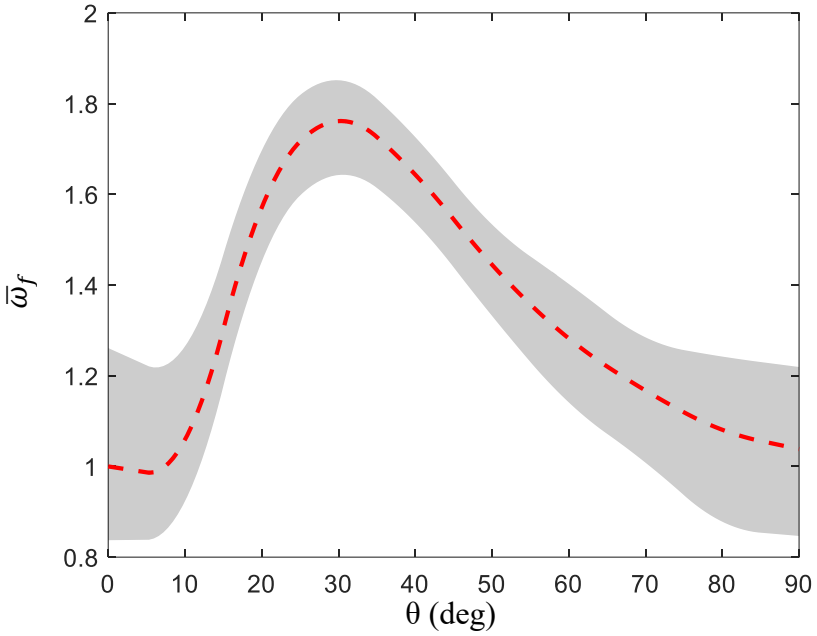

Figure 32: MCS of the baseline composite wing of case 3 for a) flutter speed b) flutter frequency

Conclusions

In this paper, the aeroelastic design and uncertainty quantification of a composite high aspect ratio wing are considered. The aeroelasticity of the wing is simulated by coupling a geometrically exact beam formulation with Peter's unsteady aerodynamic theory. It is assumed that the main load bearing part of the structure is the wing spar, and a baseline composite spar-box is designed to resemble a highly flexible wing. Three composite layups have been considered where each of them represents one of the main couplings that affect the aeroelasticity of the

wing. These layup cases are the extension-twist, lag-twist and flap twist couplings. The effects of ply angle on the flutter speed and flutter frequency for each layup have been studied. Furthermore, the effect of uniformly distributed load on the aeroelastic stability of the wing has also been investigated. It was evident that by increasing the load level, the flutter speed and frequency change depending on the ply angle and layup type. Finally, an uncertainty quantification analysis has been carried out to illustrate how the uncertainty of material properties can change the aeroelastic behaviour of the wing. It has been observed that all elastic couplings are sensitive to the uncertainty of material properties, and the maximum variation takes place at higher ply angles. It has been concluded that both flutter speed and frequency of the wing are dependent to the uncertainties of material properties. However, the layup with lag-twist coupling shows the widest variations in aeroelastic behaviour among all three layups. Finally, in future studies, a more generic wing model (with including the effects of stall) needs to be considered to investigate the effect of material uncertainties on the aeroelasticity stability of composite wings.

References

1. Afonso, F., Vale, J., Oliveira, É., Lau, F., and Suleman, A. "A review on non-linear aeroelasticity of high aspect-ratio wings," *Progress in Aerospace Sciences* Vol. 89, 2017, pp. 40-57.
2. Lucia, D. "The SensorCraft Configurations: A Non-Linear AeroServoElastic Challenge for Aviation," *46th AIAA/ASME/ASCE/AHS/ASC Structures, Structural Dynamics and Materials Conference*.
3. Romeo, G., Frulla, G., Cestino, E., and Corsino, G. "HELIPLAT: Design, Aerodynamic, Structural Analysis of Long- Endurance Solar-Powered Stratospheric Platform," *Journal of Aircraft* Vol. 41, No. 6, 2004, pp. 1505-1520.
4. Patil, M. J., and Hodges, D. H. "On the importance of aerodynamic and structural geometrical nonlinearities in aeroelastic behavior of high-aspect-ratio wings," *Journal of Fluids and Structures* Vol. 19, No. 7, 2004, pp. 905-915.
5. Cestino, E., Frulla, G., Spina, M., Catelani, D., and Linari, M. "Numerical simulation and experimental validation of slender wings flutter behaviour," *Proceedings of the Institution of Mechanical Engineers, Part G: Journal of Aerospace Engineering* Vol. 233, No. 16, 2019, pp. 5913-5928.
6. Patil, M. J., Hodges, D. H., and Cesnik, C. E. S. "Limit-cycle oscillations in high-aspect-ratio wings," *Journal of Fluids and Structures* Vol. 15, No. 1, 2001, pp. 107-132.
7. Patil, M. J., and Hodges, D. H. "Flight Dynamics of Highly Flexible Flying Wings," *Journal of Aircraft* Vol. 43, No. 6, 2006, pp. 1790-1799.
8. Calderon, D. E., Cooper, J. E., Lowenberg, M., Neild, S. A., and Coetzee, E. B. "Sizing High-Aspect-Ratio Wings with a Geometrically Nonlinear Beam Model," *Journal of Aircraft* Vol. 56, No. 4, 2019, pp. 1455-1470.
9. Hodges, D. H., and Dowell, E. H. "Nonlinear equations of motion for elastic bending and torsion of twisted nonuniform rotor blades," *NASA TN D-7818*, 1974.
10. Patil, M. J., Hodges, D. H., and Cesnik, C. E. S. "Nonlinear Aeroelasticity and Flight Dynamics of High-Altitude Long-Endurance Aircraft," *Journal of Aircraft* Vol. 38, No. 1, 2001, pp. 88-94.
11. Tang, D., and Dowell, E. H. "Experimental and Theoretical Study on Aeroelastic Response of High-Aspect-Ratio Wings," *AIAA Journal* Vol. 39, No. 8, 2001, pp. 1430-1441.
12. Tang, D., and Dowell, E. H. "Experimental and Theoretical Study of Gust Response for High-Aspect-Ratio Wing," *AIAA Journal* Vol. 40, No. 3, 2002, pp. 419-429.
13. Eaton, A. J., Howcrift, C., Coetzee, E. B., Neild, S. A., Lowenberg, M. H., and Cooper, J. E. "Numerical continuation of limit cycle oscillations and bifurcations in high-aspect-taio-wings," *Aerospace* Vol. 5, No. 3, 2018, p. 78.

14. Amato, E. M., Polsinelli, C., Cestino, E., Frulla, G., Joseph, N., Carrese, R., and Marzocca, P. "HALE wing experiments and computational models to predict nonlinear flutter and dynamic response," *The Aeronautical Journal* Vol. 123, No. 1264, 2019, pp. 912-946.
15. Duan, J. B., and Zhang, Z. Y. "Aeroelastic Stability Analysis of Aircraft Wings with High Aspect Ratios by Transfer Function Method," *International Journal of Structural Stability and Dynamics* Vol. 18, No. 12, 2018, p. 1850150.
16. Hoseini, H. S., and Hodges, D. H. "Aeroelastic Stability Analysis of Damaged High-Aspect-Ratio Composite Wings," *Journal of Aircraft* Vol. 56, No. 5, 2019, pp. 1794-1808.
17. An, C., Yang, C., Xie, C., and Yang, L. "Flutter and gust response analysis of a wing model including geometric nonlinearities based on a modified structural ROM," *Chinese Journal of Aeronautics* Vol. 33, No. 1, 2020, pp. 48-63.
18. Amoozgar, M. R., Irani, S., and Vio, G. A. "Aeroelastic instability of a composite wing with a powered-engine," *Journal of Fluids and Structures* Vol. 36, 2013, pp. 70-82.
19. Amoozgar, M. R., and Shahverdi, H. "Aeroelastic Stability Analysis of Curved Composite Blades in Hover Using Fully Intrinsic Equations," *International Journal of Aeronautical and Space Sciences*, 2019.
20. Amoozgar, M. R., Shaw, A. D., Zhang, J., and Friswell, M. I. "Composite Blade Twist Modification by Using a Moving Mass and Stiffness Tailoring," *AIAA Journal* Vol. 57, No. 10, 2019, pp. 4218-4225.
21. Amoozgar, M. R., Shaw, A. D., Zhang, J., Wang, C., and Friswell, M. I. "Lag-twist coupling sensitivity and design for a composite blade cross-section with D-spar," *Aerospace Science and Technology* Vol. 91, 2019, pp. 539-547.
22. Chattopadhyay, A., Liu, Q., and Gu, H. "Vibration Reduction in Rotor Blades Using Active Composite Box Beam," *AIAA Journal* Vol. 38, No. 7, 2000, pp. 1125-1131.
23. Farsadi, T., Rahmanian, M., and Kayran, A. "Geometrically nonlinear aeroelastic behavior of pretwisted composite wings modeled as thin walled beams," *Journal of Fluids and Structures* Vol. 83, 2018, pp. 259-292.
24. Jenett, B., Calisch, S., Cellucci, D., Cramer, N., Gershenfeld, N., Swei, S., and Cheung, K. C. "Digital Morphing Wing: Active Wing Shaping Concept Using Composite Lattice-Based Cellular Structures," *Soft Robot* Vol. 4, No. 1, 2017, pp. 33-48.
25. Librescu, L., and Song, O. *Thin-walled composite beams*. Netherland: Springer 2006.
26. Liu, X.-n., and Xiang, J.-w. "Stall Flutter Analysis of High-Aspect-Ratio Composite Wing," *Chinese Journal of Aeronautics* Vol. 19, No. 1, 2006, pp. 36-43.
27. Cesnik, C., Hodges, D., and Patil, M. "Aeroelastic analysis of composite wings," *37th Structure, Structural Dynamics and Materials Conference*.
28. Baets, P. D., Mavris, D., and Battoo, R. "Aeroelastic analysis of a composite wingbox with varying root flexibility," *41st Structures, Structural Dynamics, and Materials Conference and Exhibit*.
29. Cesnik, C., Ortega-Morales, M., and Patil, M. "Active aeroelastic tailoring of high aspect ratio composite wings," *41st Structures, Structural Dynamics, and Materials Conference and Exhibit*. Vol. AIAA-2000-1331, 2000.
30. Wang, Y., Ouyang, X., Yin, H., and Yu, X. "Structural-Optimization Strategy for Composite Wing Based on Equivalent Finite Element Model," *Journal of Aircraft* Vol. 53, No. 2, 2016, pp. 351-359.
31. Koohi, R., Shahverdi, H., and Haddadpour, H. "Nonlinear aeroelastic analysis of a composite wing by finite element method," *Composite Structures* Vol. 113, 2014, pp. 118-126.
32. Amoozgar, M. R., Fazelzadeh, S. A., Friswell, M. I., and Hodges, D. H. "Aeroelastic Stability Analysis of Tailored Pretwisted Wings," *AIAA Journal* Vol. 57, No. 10, 2019, pp. 4458-4466.
33. Amoozgar, M. R., Fazelzadeh, S. A., Haddad Khodaparast, H., Friswell, M. I., and Cooper, J. E. "Aeroelastic stability analysis of aircraft wings with initial curvature," *Aerospace Science and Technology* Vol. 107, 2020, p. 106241.
34. Amoozgar, M. R., Shaw, A. D., and Friswell, M. I. "The effect of curved tips on the dynamics of composite rotor blades," *Aerospace Science and Technology* Vol. 106, 2020, p. 106197.
35. Pettit, C. L. "Uncertainty Quantification in Aeroelasticity: Recent Results and Research Challenges," *Journal of Aircraft* Vol. 41, No. 5, 2004, pp. 1217-1229.
36. Onkar, A. K., Upadhyay, C. S., and Yadav, D. "Stochastic Finite Element Buckling Analysis of Laminated Plates With Circular Cutout Under Uniaxial Compression," *Journal of Applied Mechanics* Vol. 74, No. 4, 2006, pp. 798-809.
37. Van Vinckenroy, G., and de Wilde, W. P. "The use of Monte Carlo techniques in statistical finite element methods for the determination of the structural behaviour of composite materials structural components," *Composite Structures* Vol. 32, No. 1, 1995, pp. 247-253.
38. Lindsley, N., Beran, P., and Pettit, C. "Effects of Uncertainty on Nonlinear Plate Aeroelastic Response," *43rd AIAA/ASME/ASCE/AHS/ASC Structures, Structural Dynamics, and Materials Conference*.

39. Murugan, S., Ganguli, R., and Harursampath, D. K. "Stochastic Aeroelastic Analysis of Composite Helicopter Rotor," *Journal of the American Helicopter Society* Vol. 56, No. 1, 2011.
40. Borello, F., Cestino, E., and Frulla, G. "Structural Uncertainty Effect on Classical Wing Flutter Characteristics," *Journal of Aerospace Engineering* Vol. 23, No. 4, 2010, pp. 327-338.
41. Scarth, C., Cooper, J. E., Weaver, P. M., and Silva, G. H. C. "Uncertainty quantification of aeroelastic stability of composite plate wings using lamination parameters," *Composite Structures* Vol. 116, 2014, pp. 84-93.
42. Nitschke, C., Vincenti, A., and Chassaing, J.-C. "Influence of stochastic perturbations of composite laminate layups on the aeroelastic flutter of a cantilevered plate wing," *Composite Structures* Vol. 220, 2019, pp. 809-826.
43. Adamson, L. J., Fichera, S., and Mottershead, J. E. "Aeroelastic stability analysis using stochastic structural modifications," *Journal of Sound and Vibration* Vol. 477, 2020, p. 115333.
44. Guimarães, T. A. M., Silva, H. L., Rade, D. A., and Cesnik, C. E. S. "Aeroelastic Stability of Conventional and Tow-Steered Composite Plates Under Stochastic Fiber Volume," *AIAA Journal* Vol. 58, No. 6, 2020, pp. 2748-2759.
45. Hodges, D. H. "Geometrically Exact, Intrinsic Theory for Dynamics of Curved and Twisted Anisotropic Beams," *AIAA Journal* Vol. 41, No. 6, 2003, pp. 1131-1137.
46. Peters, D. A., Karunamoorthy, S., and Cao, W.-M. "Finite state induced flow models. I - Two-dimensional thin airfoil," *Journal of Aircraft* Vol. 32, No. 2, 1995, pp. 313-322.
47. Hodges, D. H., Atilgan, A. R., Fulton, M. V., and Rehfield, L. W. "Free Vibration Analysis of Composite Beams," *Journal of the American Helicopter Society* Vol. 36, No. 3, 1991, pp. 36-47.
48. Manan, A., and Cooper, J. "Design of Composite Wings Including Uncertainties: A Probabilistic Approach," *Journal of Aircraft* Vol. 46, No. 2, 2009, pp. 601-607.